Photooxidation of pinonaldehyde at ambient conditions investigated in the atmospheric simulation chamber SAPHIR

Michael Rolletter[1], Marion Blocquet[1,a], Martin Kaminski[1,b], Birger Bohn[1], Hans-Peter Dorn[1], Andreas Hofzumahaus[1], Frank Holland[1], Xin Li[1,c], Franz Rohrer[1], Ralf Tillmann[1], Robert Wegener[1], Astrid Kiendler-Scharr[1], Andreas Wahner[1], and Hendrik Fuchs[1]

[1]Institute of Energy and Climate Research, IEK-8: Troposphere, Forschungszentrum Jülich GmbH, Jülich, Germany
[a]now at: Ministère de l'Education Nationale et de la Jeunesse, 110 rue de Grenelle, 75357 Paris SP 07
[b]now at: Federal Office of Consumer Protection and Food Safety, Department 5: Method Standardisation, Reference Laboratories, Resistance to Antibiotics, Berlin, Germany
[c]now at: College of Environmental Sciences and Engineering, Peking University, Beijing, China

Correspondence to: Hendrik Fuchs (h.fuchs@fz-juelich.de)

Abstract. The photooxidation of pinonaldehyde, one product of the α-pinene degradation, was investigated in the atmospheric simulation chamber SAPHIR under natural sunlight at low NO concentrations (< 0.2 ppbv) with and without an added hydroxyl radical (OH) scavenger. With scavenger, pinonaldehyde was exclusively removed by photolysis, whereas without scavenger, the degradation was dominated by reaction with OH. In both cases, the observed rate of pinonaldehyde consumption was faster than predicted by an explicit chemical model, the Master Chemical Mechanism (MCM, version 3.3.1). In the case with OH scavenger, the observed photolytic decay can be reproduced by the model, if an experimentally determined photolysis frequency is used instead of the parameterization in the MCM. A good fit is obtained, when the photolysis frequency is calculated from the measured solar actinic flux spectrum, absorption cross-sections published by Hallquist et al. (1997), and an effective quantum yield of 0.9. The resulting photolysis frequency is 3.5 times faster than the parameterization in the MCM. When pinonaldehyde is mainly removed by reaction with OH, the observed OH and hydroperoxy radical (HO_2) concentrations are underestimated in the model by a factor of 2. Using measured HO_2 as a model constraint brings modeled and measured OH concentrations into agreement. This suggests that the chemical mechanism includes all relevant OH producing reactions, but is missing a source for HO_2. The missing HO_2 source strength of $(0.8 \text{ to } 1.5)\,\mathrm{ppbv}\,h^{-1}$ is similar to the rate of the pinonaldehyde consumption of up to $2.5\,\mathrm{ppbv}\,h^{-1}$. When the model is constrained by HO_2 concentrations and the experimentally derived photolysis frequency, the pinonaldehyde decay is well represented. The photolysis of pinonaldehyde yields 0.18 ± 0.20 formaldehyde molecules at NO concentrations of less than $200\,\mathrm{pptv}$, but no significant acetone formation is observed. When pinonaldehyde is also oxidized by OH under low NO conditions (maximum $80\,\mathrm{pptv}$), yields of acetone and formaldehyde increase over the course of the experiment from 0.2 to 0.3 and from 0.15 to 0.45, respectively. Fantechi et al. (2002) proposed a degradation mechanism based on quantum-chemical calculations, which is considerably more complex than the MCM scheme and contains additional reaction pathways and products. Implementing these modifications results in a closure of the model-measurement discrepancy for the products acetone and formaldehyde, when pinonaldehyde is degraded only by photolysis. In contrast, the underprediction of formed acetone and formaldehyde is worsened compared to model results by the MCM,

when pinonaldehyde is mainly degraded in the reaction with OH. This shows that the current mechanisms lack acetone and formaldehyde sources for low NO conditions like in these experiments. Implementing the modifications suggested by Fantechi et al. (2002) does not improve the model-measurement agreement of OH and HO_2.

1 Introduction

Globally, emissions of biogenic non-methane volatile organic compounds (NMVOCs) in the atmosphere are ten times higher than emissions of anthropogenic NMVOCs (Guenther et al., 2012). Of these emissions, monoterpenes (C10-compounds) represent approximately 15 % (Guenther et al., 2012) of the total emissions. Monoterpenes are mainly oxidized in the atmosphere by ozonolysis or their reaction with the hydroxyl radical (OH) during daytime. However, also oxidation by the nitrate radical (NO_3) during nighttime can be of importance enhanced by nocturnal monoterpene emissions (Calogirou et al., 1999; Atkinson and Arey, 2003). Oxidation products significantly contribute to the global production of, for example, acetone (Jacob et al., 2002). In addition, low-volatile organic oxidation products play an important role for the formation of secondary organic aerosol (SOA) (Kanakidou et al., 2000). The oxidation of monoterpenes and their oxidation products is also of importance for the tropospheric ozone production (Schwantes et al., 2020).

Field measurements indicate that there is a lack of understanding of the radical chemistry connected to the photooxidation of monoterpenes (e.g. Peeters et al., 2001; Capouet et al., 2004, and references therein). Hydroperoxy radical (HO_2) concentrations measured in environments dominated by monoterpenes are not well-understood by model calculations, for example in a campaign performed in the foothills of the Rocky Mountains (Kim et al., 2013) and in a boreal forest in Finland (Hens et al., 2014). In these campaigns, modeled HO_2 concentrations were lower by a factor of 2 and 2.5, respectively, compared to measurements. Also chamber studies, investigating the oxidation of α- and β-pinene gave higher HO_2 concentrations than model calculations suggest (Kaminski et al., 2017; Rolletter et al., 2019).

Among the monoterpenes, α-pinene is the most abundant one (Guenther et al., 2012). Pinonaldehyde is one of the first-generation oxidation products. In the α-pinene photooxidation, initially 3 different peroxy radicals (RO_2) are formed and 2 of them eventually form pinonaldehyde. Several field campaigns reported pinonaldehyde concentrations measured on filter samples (Kavouras et al., 1999; Alves et al., 2002; Boy et al., 2004; Cahill et al., 2006; Rissanen et al., 2006; Herckes et al., 2006; Plewka et al., 2006) or in the analysis of rain and snow samples (Satsumabayashi et al., 2001). Only few studies reported ambient gas phase concentrations of pinonaldehyde. Field studies in the San Bernardino National Forest, California (Yu et al., 1999) and the German Fichtelgebirge (Müller et al., 2006) reported pinonaldehyde concentrations in the gas phase of approximately 0.15 ppbv. Another study by Cahill et al. (2006) conducted in the Sierra Nevada Mountains of California measured 0.05 to 0.30 ppbv gaseous pinonaldehyde. Pinonaldehyde yields from the photochemical degradation of α-pinene with OH were measured in laboratory experiments ranging from 6 to 87 % (Larsen et al., 2001; Noziére et al., 1999). The high variability could be due to different chemical conditions with partly high reactant concentrations used in these experiments. A recent study in the atmospheric simulation chamber SAPHIR used ambient reactant concentrations ([α-pinene] ≤ 3.8 ppbv, [NO] < 120 pptv, (310 ± 5) K) and reported a low yield of 5 % (Rolletter et al., 2019). As currently implemented in the Master Chemical Mechanism (MCM, 2017; Jenkin et al., 1997; Saunders et al., 2003) pinonaldehyde is formed with a total yield of 84 %. In contrast, a theory based study by Vereecken et al. (2007) suggested a different branching ratio of initial RO_2 and additional reaction channels which lead in total to pinonaldehyde yields of 60 % for low atmospheric NO conditions (≤ 1 ppbv NO). Our previous study (Rolletter et al., 2019) showed that further adjustment of the initial RO_2 branching ratio in a mecha-

nism based on Vereecken et al. (2007) was necessary to explain the low measured pinonaldehyde yield of 5 % for conditions similar to the experiments discussed here. A similar change in RO_2 branching ratios was found in an experimental study by Xu et al. (2019).

The photochemistry of pinonaldehyde has been investigated in only few experimental studies (Noziére et al., 1999; Jaoui and Kamens, 2003; Capouet et al., 2004) in addition to few theoretical studies (Glasius et al., 1997; Vereecken and Peeters, 2002; Fantechi et al., 2002; Dash and Rajakumar, 2012). The pinonaldehyde degradation during daytime is controlled by photolysis and the reaction with OH radicals resulting in an atmospheric lifetime on the order of a few hours due to its fast reaction with OH (Atkinson et al., 2004). The lifetime of pinonaldehyde with respect to photodissociation strongly depends on the season and the latitude, but can be comparable to the reaction with OH (Hallquist et al., 1997). Main oxidation products (Fig. 1) of the photolysis and OH reactions are norpinonaldehyde (NORPINAL; names are taken from the MCM), pinonic acid (PINONIC), perpinonic acid (PERPINONIC), formaldehyde (HCHO), and acetone. So far, there has been only one study by Noziére et al. (1999) reporting yields for the reaction with OH for HCHO and acetone of (152 ± 56) % and (15 ± 7) %, respectively.

A simplified oxidation scheme of pinonaldehyde is shown in Fig. 1. As implemented in the MCM, the photolysis of pinon-aldehyde (PINAL) leads to dissociation in HCO and an organic radical, both of which react with O_2 to form CO, HO_2 and the peroxy radical C96O2.

$$PINAL + h\nu + O_2 \quad \rightarrow \quad C96O2 + CO + HO_2 \tag{R1}$$

The oxidation of pinonaldehyde by OH is initiated by H-abstraction mainly at the aldehyde group forming primary RO_2. In the MCM, an acyl peroxy radical (C96CO3) and PINALO2 are formed.

$$PINAL + OH + O_2 \quad \rightarrow \quad C96CO3 \quad (\text{yield} : 0.77) \tag{R2}$$
$$PINAL + OH + O_2 \quad \rightarrow \quad PINALO2 \quad (\text{yield} : 0.23) \tag{R3}$$
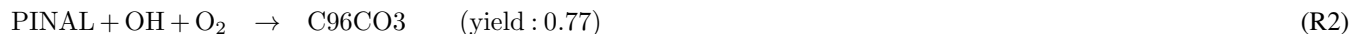
In the presence of high nitric oxide (NO) concentrations, RO_2 react with NO and form either alkoxy radicals (RO) or organic nitrate compounds ($RONO_2$). In the reaction forming an alkoxy radical, NO is converted to NO_2 and HO_2 to OH, respectively. The alkoxy radical subsequently reacts with O_2 to form a carbonyl compound and HO_2, decomposes or isomerizes. At low NO concentrations, RO_2 reactions with HO_2 terminating the radical chain reactions and forming stable hydroxyperoxides (ROOH) gain in importance. Formed stable organic products of $RO_2 + NO$ and $RO_2 + HO_2$ reactions can further react with OH or photolyse.

The reaction of the most important RO_2 radical, C96CO3 with HO_2 can either directly form the same product (C96O2) as its reaction with NO or can form the stable products pinonic and perpinonic acid. Subsequently, pinonic and perpinonic acid are photolyzed or react with OH and thereby producing again the peroxy radical C96O2. Similarly, other $RO_2 + HO_2$ reactions not shown in Fig. 1 produce the same species which are produced by $RO_2 + NO$ reactions.

In the atmosphere, the peroxy radical C96O2 can react with nitric oxide (NO) to form the corresponding alkoxy radical C96O.

$$C96O2 + NO \quad \rightarrow \quad C96O + NO_2 \tag{R4}$$

C96O undergoes isomerization or decomposition reactions producing formaldehyde, acetone or 3,4-dioxopentanal (CO23C4CHO).

The main products of the subsequent chemistry of the other peroxy radical PINALO2, including multiple reactions with NO and decomposition reactions, are HO_2, a tri-carbonyl compound, acetone, and formaldehyde.

5   In contrast to the MCM, the theoretical study by Fantechi et al. (2002) predicts other decomposition reactions of products of the $RO_2 + NO$ reaction (Fig. 1). Whereas other theory based studies investigated the reaction rate of pinonaldehyde + OH (Glasius et al., 1997) and the probability of H-abstraction by OH at various sites of pinonaldehyde (Vereecken and Peeters, 2002; Dash and Rajakumar, 2012), Fantechi et al. (2002) analysed also the subsequent chemistry of the initially formed organic peroxy radicals. Instead of forming acetone and formaldehyde in the further degradation of C96O, Fantechi et al. (2002)
10 suggest that the the main fraction of C96O undergoes a series of isomerization reactions and reactions with NO forming 4-hydroxynorpinonaldehyde. In contrast to the MCM, the four-membered ring structure is retained in the formed products. A small fraction (~ 7%) directly forms norpinonaldehyde (NORPINAL) after H-abstraction by O_2. The modifications by Fantechi et al. (2002) are limited to $RO_2 + NO$ chemistry and no detailed analysis of $RO_2 + HO_2$ reactions was done in their work. Nevertheless, modifications suggested by Fantechi et al. (2002) also affect $RO_2 + HO_2$ chemistry, if products from these
15 reactions are the same as from the reaction of $RO_2 + NO$ as implemented in the MCM. In the model by Fantechi et al. (2002) some $RO_2 + NO$ reactions also lead to the formation of organic nitrates with yields between 14 % and 28 %, which lower the yield of formed HO_2 and carbonyl compounds.

    Fantechi et al. (2002) proposed two additional relevant (yields > 5 %) peroxy radicals formed by the initial OH attack. Accordingly, the yields of C96CO3 and PINALO2 are changed from 77 % to 61 % and 23 % to 9 % compared to the MCM,
20 respectively. The first additional reaction channel with a branching ratio of 24 % leads to a formation of norpinonaldehyde. The second additional reaction channel with only a minor contribution of 6 % forms in the subsequent chemistry acetone, formaldehyde and a tri-carbonyl-hydroxy compound.

    In this work, the photochemistry of pinonaldehyde was investigated under controlled, atmospheric conditions including atmospherically reactant concentrations and natural sunlight in the outdoor chamber SAPHIR (Simulation of Atmospheric
25 PHotochemistry In a large Reaction Chamber) at Forschungszentrum Jülich. This study focusses on (a) the determination of the pinonaldehyde photolysis frequency, (b) quantification of HO_x (= OH + HO_2) radicals in the OH–oxidation of pinonalde-hyde, and (c) the determination of acetone and formaldehyde yields of both photolysis and OH–oxidation. Measurements of pinonaldehyde, degradation products and HO_X radicals are compared to model calculations applying the Master Chemical Mechanism v3.3.1. Sensitivity model runs are performed including reaction pathways and yields suggested by the theoretical
30 study of Fantechi et al. (2002) and the impact of the proposed mechanism on concentrations of organic compounds and HO_x radicals is analyzed.

2 Methods

2.1 Atmospheric simulation chamber SAPHIR

Details of the SAPHIR chamber can be found elsewhere (e.g. Rohrer et al., 2005; Bohn et al., 2005) and the chamber is only briefly described here. It is of cylindrical shape (18 m length, 5 m diameter, and 270 m^3 volume) and is made of a double wall FEP film. The FEP ensures inertness of the surfaces and minimizes wall effects. This outdoor chamber allows studying the photochemical reactions under natural sunlight, because the FEP film is transmissive for the entire solar spectrum. The chamber is equipped with a shutter system that can shield the chamber from sunlight.

Ultra-pure synthetic air used in the experiments is mixed from liquid nitrogen and oxygen (Linde, purity >99.9999 %). The pressure inside the chamber is slightly (30 Pa) above ambient pressure to prevent impurities from ambient air leaking into the chamber. Air that is consumed by instruments or is lost due to small leakages is replenished to keep a constant pressure. The replenishment flow is in the range of 9 to 12 m^{3}h^{-1} leading to a dilution of trace gases of 3 to 4 % h^{-1}. Rapid mixing of air is ensured by the operation of two fans inside the chamber.

In the sunlit chamber, there are small sources for nitrous acid (HONO), formaldehyde (HCHO), and acetone. Their formation rates depend on the intensity of solar radiation, relative humidity and temperature (Rohrer et al., 2005). The photolysis of HONO is the major primary source for nitrogen oxides and OH. Approximately, 250 pptv h^{-1} NO$_x$, 200 pptv h^{-1} HCHO and 100 pptv h^{-1} acetone were formed in the experiments in this study.

2.2 Instrumentation

An overview of used instruments and their 1 σ accuracies and precision is given in Table 1.

OH radicals were measured by laser induced fluorescence (LIF). The instrument operated at the SAPHIR chamber has been described elsewhere (e.g. Holland et al., 2003; Fuchs et al., 2012). Chamber air is sampled through an inlet nozzle into a low-pressure measurement cell, where OH is excited by pulsed laser radiation at 308 nm. Its fluorescence is subsequently detected by gated photon counting. In addition, HO$_2$ radicals are indirectly detected after chemical conversion to OH by NO in another measurement cell (Fuchs et al., 2011). The instrument is calibrated by a radical source, in which OH and HO$_2$ are produced by water vapor photolysis at 185 nm (Fuchs et al., 2011).

Interferences can occur in the HO$_2$ measurements because of concurrent conversion of specific RO$_2$ radicals which produce OH in the reaction with NO on a similar time scale as HO$_2$ does (Fuchs et al., 2011; Whalley et al., 2013; Lew et al., 2018). Because the conversion of RO$_2$ requires at least two reaction steps with NO in contrast to HO$_2$ for which only one reaction step leads to the formation of OH, this interference can be minimized, if the conversion efficiency of HO$_2$ is below 10 %. This can be achieved by adjusting the NO concentration in the HO$_2$ cell. This was done in this study, so that it can be assumed that potential interferences in the HO$_2$ detection were negligible.

In addition, OH was measured by differential optical absorption spectrometry (DOAS; Dorn et al., 1995b) which is an absolute measurement technique. Measured OH concentrations of both instruments agreed on average within 15 % similar to results in previous experiments (Fuchs et al., 2012).

Organic compounds were measured by proton transfer reaction time-of-flight mass spectrometry (PTR-TOF-MS; Lindinger et al., 1998; Jordan et al., 2009) and by gas chromatography that was coupled to a flame ionization detector (GC-FID). Formaldehyde was measured by a Hantzsch instrument and by DOAS.

Photolysis frequencies (j) of NO_2, HONO, O_3, and pinonaldehyde were calculated from actinic flux density spectra that are derived from measurements of total and diffuse spectral actinic flux densities outside the chamber. From these measurements direct sun contributions are calculated. The direct and diffuse actinic flux densities are used as input for a model which calculates mean chamber spectra by taking into account the time-dependent effects of shadings of the chamber steel frame and the transmittance of the Teflon film which is > 0.8 in the complete solar spectral range (Bohn and Zilken, 2005). Mean photolysis frequencies are then calculated by the following equation:

$$j = \int \sigma(\lambda)\phi(\lambda)F_\lambda(\lambda)d\lambda \qquad (1)$$

with σ the absorption cross section, ϕ the quantum yield, and F the actinic flux. The absorption cross sections and quantum yields of NO_2, HONO, and O_3 used for the calculations of photolysis frequencies are taken from the literature (Mérienne et al., 1995; Troe, 2000; Stutz et al., 2000; Daumont et al., 1992; Matsumi et al., 2002). The method is regularly evaluated by dedicated experiments using the chamber as a chemical actinometer (Bohn et al., 2005). The pinonaldehyde photolysis frequency is discussed in more detail in Section 4.1.

NO and NO_2 were measured by chemiluminescence (Eco Physics), water vapor mixing ratios by a cavity ring-down instrument (Picarro) and ozone (O_3) by an UV absorption instrument (Ansyco).

2.3 Experimental procedure

Before the experiment, the chamber was flushed with dry, synthetic air to dilute trace gases from previous experiments below the detection limits of the instruments. Twenty ppm of CO_2 was injected as a dilution tracer in the beginning of each experiment. Water from a Milli-Q-device was boiled and flushed into the chamber together with a high flow of synthetic air ($150\,m^3h^{-1}$). The chamber was only humidified in the beginning of an experiment reaching initial water vapor concentrations of about 2 % which decreased over the course of an experiment due to the dilution with dry synthetic air.

Pinonaldehyde (Orgentis chemicals, 98.2 %) was heated in a glass vial and the vapor was flushed together with a small flow of dry nitrogen into the chamber using a short Teflon tube. After the injection had been stopped, the sample line was removed to avoid further evaporation of pinonaldehyde from the injection system into the chamber. The initial pinonaldehyde concentrations were 6.5 and 16.5 ppbv in the experiments on 17 July and 18 July 2014, respectively. The chamber roof was opened after a stable pinonaldehyde concentration was observed by the PTR-TOF-MS instrument.

In one experiment (18 July 2014), 2500 ppbv of cyclohexane was additionally injected after the humidification. Cyclohexane served as scavenger for OH in this experiment in order to study the pinonaldehyde photolysis independently from its reaction with OH.

In the other experiment (17 July 2014), 70 ppbv of ozone produced from a silent discharge ozonizer (O3Onia) was injected after humidification, so that a low NO concentration (maximum 80 pptv) was obtained during the experiment. In this experi-

ment, approximately 20 % of reacted pinonaldehyde was photolyzed and the remaining 80 % reacted with OH. The reaction of pinonaldehyde with ozone is very slow ($k = (8.9 \pm 1.4) \times 10^{-20} \text{cm}^3\text{s}^{-1}$, Glasius et al. (1997)) and therefore ozonolysis reactions did not play a role in the experiments here.

2.4 Model calculations

The Master Chemical Mechanism (MCM) in its latest version 3.3.1 was applied as base model for box model calculations (MCM, 2017; Jenkin et al., 1997; Saunders et al., 2003). FACSIMILE was used as solver for differential equations in the model calculations.

In order to account for chamber effects, the following modifications were added to the MCM model. Dilution to all trace gases was applied. The dilution rate was calculated from the monitored replenishment flow rate that was consistent with the dilution of the CO_2 tracer. Small chamber sources of formaldehyde and acetone were parameterized based on reference experiments as described in Rohrer et al. (2005); Karl et al. (2006); Kaminski et al. (2017).

Temperature, pressure, H_2O, NO, NO_2, HONO, and O_3 concentrations were constrained to measured values. These constrains were used because chamber NO sources cannot be modeled accurately and therefore could lead to wrong conclusions in the analysis of turnover rates of radicals.

Photolysis frequencies, which were not measured, were calculated for clear sky conditions by the parameterization included in the MCM. They were scaled to take cloud cover and the transmission of the Teflon film into account by the ratio of measured to modeled photolysis frequency of NO_2. This applies also for the photolysis frequency of pinonaldehyde in the base model case (MCM). All other model runs used the experimentally derived pinonaldehyde photolysis frequency (see Section 4.1).

The injection of pinonaldehyde was modeled as a source only present during the time period of injection to match the pinonaldehyde increase as measured by PTR-TOF-MS.

In a sensitivity study, the pinonaldehyde oxidation scheme developed by Fantechi et al. (2002) was implemented. In this mechanism, additional reaction pathways of the pinonaldehyde reaction with OH that are not included in the MCM are suggested. Only the four reaction pathways with significant yields ($> 5 \%$) were implemented for the sensitivity model run (Fig. 1). In addition, the fate of the most abundant RO_2 formed from the reaction of pinonaldehyde with OH or photolysis is different in this model compared to the MCM mechanism (see above). Reaction rate constants and branching ratios were used as described in Fantechi et al. (2002). Simple rate coefficients such as KDEC ($= 1 \times 10^6$) and KRO2NO ($= 2.7 \times 10^{-12}$ exp(360/T)) from the MCM were used, when no specific reaction rate constants were mentioned. To account for possible $RO_2 + HO_2$ reactions, a reaction scheme based on the reaction C97O2 + HO_2 was added for all newly introduced RO_2 species not included in the MCM. $RO_2 + HO_2$ reactions form a corresponding hydroxyperoxide (ROOH) that can either react with OH to regenerate the RO_2 or photolyse to form the corresponding alkoxy radical (RO). Modifications by Fantechi et al. (2002) describe the chemistry from the OH attack on pinonaldehyde until the formation of stable products 4-hydroxynorpinonaldehyde, norpinonaldehyde, CO23C4CHO, and C818CO. The chemistry of the products norpinonaldehyde, CO23C4CHO and C818CO was treated as described in the MCM. For 4-hydroxynorpinonaldehyde, no follow-up chemistry was considered.

Both MCM and Fantechi et al. (2002) mechanism were tested under different conditions. An overview of used model calulations is given in Table 2.

3 Results

Figures 2 and 3 show the concentration time series of pinonaldehyde and other measured trace gases together with MCM model results for the two experiments with and without OH scavenger, respectively.

Weather conditions were similar for both experiment days. The temperature inside the chamber increased over the course of each experiment from 305 to 315 K. The solar zenith angle at noon was $30\,^\circ$ and maximum measured pinonaldehyde photolysis frequencies were approximately $3.5\,x\,10^{-5}\ s^{-1}$ in both experiments.

In both experiments, the measured pinonaldehyde decay was significantly faster than predicted by the model once the chamber roof was opened. The predicted pinonaldehyde consumption rate was slower by 50 % and 25 % in the pure photolysis case and in the OH oxidation case, respectively. Potential wall loss of pinonaldehyde in the chamber was tested in separate experiments, in which pinonaldehyde was injected into the dark chamber. The loss of pinonaldehyde in this case is consistent with the dilution calculated from the replenishment flow.

Also the two measured major organic products, acetone and formaldehyde, are not well reproduced by the model calculations. In the experiment with the OH scavenger, in which pinonaldehyde is removed by photolysis only, the modeled concentrations of formaldehyde and acetone are 60 % and 70 % higher compared to the measurements, although the photolysis frequency of pinonaldehyde is obviously underestimated. In contrast, in the experiment in which pinonaldehyde was photolyzed and oxidized by OH modeled acetone concentrations are underestimated by 17 % compared to measurements. Modeled formaldehyde concentrations are 6 % smaller than measurements, which is within the measurement uncertainty. The smaller modeled acetone yield cannot be explained only by the lower consumption of pinonaldehyde in the model. A sensitivity run which reproduces the pinonaldehyde consumption also underestimates the acetone concentrations.

In the experiment without scavenger, OH and HO_2 are both considerably underpredicted by the MCM. While OH shows an increasing discrepancy of up to a factor of 2, modeled HO_2 is a factor of 2–4 lower than measured. In the experiment with OH scavenger, measured and modeled HO_2 concentrations agree within the stated uncertainty during the first part of the experiment, but the model underestimates the HO_2 by 50 % in the last hour.

Measured time series of acetone and formaldehyde are used to determine the total yields of acetone and formaldehyde from the pinonaldehyde oxidation following the procedure described by Galloway et al. (2011), Kaminski et al. (2017), and Rolletter et al. (2019). In this approach, the measured time series of trace gases are corrected for loss and production that are not directly related to the chemical oxidation scheme of pinonaldehyde. This includes dilution of trace gases in the chamber, loss of formaldehyde due to photolysis and small production of formaldehyde and acetone in the sunlit chamber that is independent from the pinonaldehyde chemistry. If also OH is present, additional corrections for the losses of formaldehyde and acetone due to their reactions with OH are applied. The corrected time series can then be used to calculate the ratio of a formed organic product and the consumed pinonaldehyde to derive the yield of the organic compound that is connected to the chemical

degradation of pinonaldehyde. The main uncertainty in the calculated yields is caused by the uncertainty of the strength of the small chamber sources which has to be taken from characterization experiments that were performed before/after the experiments with pinonaldehyde. Sensitivity studies in which the source strengths are systematically varied show that 1σ uncertainties of yields are 0.2 and 0.1 for formaldehyde and acetone, respectively.

5   Figure 4 shows the result of the yield calculations. The formaldehyde yield is (0.1 ± 0.2) in the beginning and increases to approximately (0.18 ± 0.2) in the end of the experiment. The acetone yield of the photolysis is zero within the uncertainty of 0.1.

    The yields of acetone and formaldehyde are also calculated from the measured time series in the experiment when pinonaldehyde was oxidized by OH as described for the experiment with OH scavenger. Results are shown in Fig. 5. The yields of
10   both species increase over the course of the experiment. The formaldehyde yield increases from approximately (0.15 ± 0.2) to values higher than (0.45 ± 0.2) and the acetone yield from approximately (0.2 ± 0.1) to (0.3 ± 0.1).

4   Discussion

4.1   Pinonaldehyde photolysis

In the presence of an OH scavenger, the pinonaldehyde decay observed in the chamber could be due to photolysis, wall loss
15   and dilution. As was shown by additional experiments in the dark chamber, wall loss is negligible on the time scale of a few hours. The effect of dilution was quantified from the measured dilution flow rate and the chamber volume and agreed with the results from the tracer (CO_2) measurements within 3 %. Without OH, the chemical degradation of pinonaldehyde depends only on the photolysis frequency of pinonaldehyde. In MCM, photolysis frequencies are generally calculated as a function of solar zenith angle χ using three parameters l, m, and n.

$$J = l \cdot (\cos(\chi))^m \cdot e^{(-n \cdot \sec(\chi))} \tag{2}$$

For pinonaldehyde, MCM is using the parameters (l = 2.792×10^{-5}s^{-1}, m = 0.805, n = 0.338; valid for clear sky conditions) for the photolysis of n-butanal. The parameterization is based on the absorption spectrum measured for n-butanal at 298 K by Martinez et al. (1992) and the quantum yield (0.21) for its dissociation to n-C$_3$H$_7$ + HCO at 298 K and 1 atm by Tadić et al. (2001). For the evaluation of the chamber experiments, the clear sky values from the parameterization (Equation 1) are
25   corrected for the influence of cloud cover and chamber transmission by multiplying the clear sky value by the ratio of the measured to parametrized photolysis frequency of NO$_2$. Following this procedure, the simulated decay of pinonaldehyde in the base model (MCM) is considerably slower than the observed decay (Fig. 6).

    As an alternative, the photolysis frequency of pinonaldehyde is calculated using the measured spectrally-resolved solar actinic flux (Section 2.2) and the pinonaldehyde absorption spectrum (280-340 nm) measured at 300 K by Hallquist et al. (1997).
30   Good agreement between the observed and simulated (MCM_a) pinonaldehyde decay is achieved, if an effective quantum yield of 0.9 is assumed (Fig. 6, upper panel). Here, the mean decay rate of pinonaldehyde between 10:00 and 15:00 (UTC) is 3.9 x 10^{-5} s^{-1}, of which 2.9 x 10^{-5} s^{-1} is caused by photolysis and 1.0 x 10^{-5} s^{-1} by dilution. The experimentally derived

photolysis frequencies are approximately a factor of 3 to 3.5 higher than the values from the parameterization in the MCM. The experimental error (20 %) of the effective quantum yield (0.9) is mainly determined by the uncertainties of the absorption spectrum (< 5 %; Hallquist et al. (1997)) and the actinic flux measurement (10 %). Error contributions from wall loss and dilution are small (< 5 %).

5   The applied absorption cross sections by Hallquist et al. (1997) are the only published measurements and are recommended by IUPAC (Atkinson et al., 2006). The effective, wavelength-independent quantum yield determined in this work is significantly higher than in two other chamber studies, which report values of 0.14 ± 0.03 (Moortgat et al., 2002) and 0.4 (Jaoui and Kamens, 2003) for photolysis with natural sunlight. No recommendation for the quantum yield is given by IUPAC (Atkinson et al., 2006). Both chamber studies applied the absorption spectrum from Hallquist et al. (1997) for the calculation of photolysis

10   frequencies. Jaoui and Kamens (2003) measured the solar radiation by a UV-Eppley radiometer. The broadband instrument measures the spectrally integrated solar irradiance (spatially cosine-weighted photon-flux density) from 300 nm to 400 nm. The non-trivial conversion to a actinic flux spectrum (spatially isotropically weighted photon-flux density) between 300 nm and 340 nm needed for the evaluation of the pinonaldehyde photoloysis frequencies has not been documented by the authors. The conversion requires knowledge of the spatial distribution of the incident solar radiation, which is a function of solar zenith

15   angle, wavelength, atmospheric aerosol and clouds (Hofzumahaus, 2006). Furthermore, the wavelength range of pinonaldehyde photolysis (< 340 nm) strongly depends on the total atmospheric ozone column, while UV Eppley measurements (300-400 nm) are only weakly dependent on total ozone. Considerable errors may therefore be connected to the conversion of Eppley data to photolysis frequencies for pinonaldehyde.

     In the study by Moortgat et al. (2002), solar actinic flux was directly measured by a spectroradiometer with good accuracy

20   like in the present work. However, similar to Jaoui and Kamens (2003), Moortgat et al. (2002) had to apply large corrections for wall losses and dilution, each of which were of the same magnitude as the photolysis rate. The large difference by a factor of 7 in comparison to the present work is likely not explained by systematic errors of the correction.

     The pinonaldehyde photolysis is faster than n-butanal because of its two carbonyl functions. This might be valid for other bi-carbonyl compounds that have non-conjugated carbonyl functions, so that the use of the n-butanal photolysis frequency

25   could systematically underestimate the photolysis frequencies of these compounds. However, the high quantum yield close to unity could also be a specific property of pinonaldehyde that might not apply for the photolysis of other bi-carbonyl species.

     Figure 4 shows the time series of measured acetone and formaldehyde concentrations together with results from model calculations applying the MCM. In contrast to the base case model (MCM, Fig. 2), measured photolysis frequencies are used (MCM_a). As a consequence of the the higher photolysis frequencies, the consumption of pinonaldehyde leads to even larger

30   productions of formaldehyde and acetone (approximately three times higher than measured values) compared to the base case model.

     For conditions of this experiment, 80 % of RO_2 radicals formed in the photolysis reaction of pinonaldehyde are reacting with NO and only 20 % are reacting with HO_2, so that carbonyl compounds are expected to be the main organic products (Fig. 1). Acetone measured in this experiment is solely formed by the chamber source. Initial acetone yield values are negative

35   because of the high uncertainty in the corrections that are applied in the yield calculation. In the beginning of an experiment,

only small amounts of products are formed which leads to a large uncertainty, so that negative values are not significant. It has to be stressed here again that the parametrization of the chamber source is the main uncertainty in the yield calculation. If the chamber source was overestimated, the constant measured acetone yield could also include a small contribution from the pinonaldehyde photolysis.

5   In a sensitivity model run (FAN_a), the pinonaldehyde oxidation scheme suggested by Fantechi et al. (2002) is tested for the experiment with OH scavenger. While the initial photodissociation step and the reaction of C96O2 with NO are the same, the following decomposition of C96O yields considerably different organic products. No acetone and less formaldehyde are produced together with mainly 4-hydroxynorpinonaldehyde and norpinonaldehyde that were not measured in these experiments. Agreement between modeled and measured acetone is achieved within the accuracy of measurements of 10 %. Also

10   modeled formaldehyde concentrations are only 20 % lower than measured values. Thus, the model description of acetone and formaldehyde products is greatly improved by the use of the Fantechi et al. (2002) mechanism compared to the MCM.

To our knowledge, there is only one other study by Jaoui and Kamens (2003), which investigated the product yields of pinonaldehyde photolysis. Products were measured by gas-chromatography in that chamber study in the presence and absence of an OH scavenger. The measured norpinonaldehyde yield agrees within the stated uncertainty with the yield proposed by

15   Fantechi et al. (2002). Formaldehyde and acetone yields were not measured by Jaoui and Kamens (2003).

Using the MCM with the measured photolysis frequency (MCM_a) leads to an increase in modeled HO_2 of about 25 % (Fig. 6, lower panel) which can be explained by the higher amount of consumed pinonaldehyde that is formed at the end of the radical reaction chain together with 3,4-dioxopentanal (CO23C4CHO). Unfortunately, between 11:30 and 14:00 experimental problems occurred in the HO_2 measurements. Neither NO measurements nor photolysis frequencies showed any features

20   that could explain the decrease in the HO_2 concentration. The exact reason of the HO_2 variations remains unclear and the uncertainty of HO_2 measurements is likely higher (50 %) for this period. Implementing the modifications by Fantechi et al. (2002) results in a HO_2 concentration time profile (FAN_a) that is different from both model runs done with the MCM mechanism. In the FAN_a model run HO_2 is formed more rapidly compared to the MCM and concentrations decrease towards the end of the experiment. The rate determining step in radical chain reactions is the reaction of RO_2 with NO forming an

25   alkoxy radical and NO_2. In the MCM, there are 3 $RO_2 + NO$ reactions before the radical chain is terminated and the stable product CO23C4CHO is formed together with HO_2. In contrast, in the Fantechi et al. (2002) mechanism only one $RO_2 + NO$ reaction occurs before the stable products are formed and HO_2 is regenerated. In addition, no subsequent chemistry of the formed product 4-hydroxynorpinonaldehyde is included in the model which would produce additional HO_2, especially in later stages of the experiment.

30 **4.2   Photooxidation by OH**

In the photooxidation experiment without OH scavenger (Fig. 3), a much faster decay of pinonaldehyde is observed compared to the case with OH scavenger (Fig. 2). Without scavenger, 30 % of the decay in the beginning of the experiment is explained by photolysis and 5 % by dilution. The remaining 65 % are due to the removal of pinonaldehyde by OH. However, OH concentrations rise over the course of the experiment and the pinonaldehyde fraction reacting with OH increase to up to 80 %. Here

and in the following analysis, experimental photolysis frequencies are used, which assume a quantum yield of 0.9 (see Section 4.1). The photolysis and the OH reaction of pinonaldehyde lead to a mix of peroxy radicals (Fig. 1), which react mainly with HO_2 or NO. During the experiment, the NO mixing ratio increases from about 10 pptv to 80 pptv. Accordingly, the fraction of RO_2 radicals reacting with NO increases from 20 % to 55 %, while the RO_2 fraction reacting with HO_2 decreases.

5   Applying the experimental pinonaldehyde photolysis frequency to the model (MCM_a) improves the simulation of the pinonaldehyde decay compared to the base model run (MCM), which uses a slower parameterized photolysis frequency. However, even with the faster photolysis rate, the consumption of pinonaldehyde is underestimated (Fig. 7, upper panel). At the end of the experiment (15:00), the remaining modeled pinonaldehyde concentration is a factor of 2 larger than the measured value. This is due to the lower OH concentration in the model compared to measurements. If modeled OH concentrations are

10 increased to match measured values, which can be achieved by constraining HO_2 in the model to measurements (MCM_b), modeled and measured pinonaldehyde concentrations agree within 10 % (Fig. 7). This demonstrates that missing OH production in the model is most likely due to the underestimation of HO_2, which forms OH by reaction with NO. This suggests that there is a HO_2 source missing in the model. In a sensitivity run (not shown here) artificial HO_2 sources were added to the model to quantify the required HO_2 source strength. The missing HO_2 source is increasing over the course of the experiment.

15 A source strength between $0.8\,\mathrm{ppbv\,h^{-1}}$ and $1.5\,\mathrm{ppbv\,h^{-1}}$ would be required to explain observations. The consumption of pinonaldehyde during the experiment is up to $2.5\,\mathrm{ppbv\,h^{-1}}$, so that a comparably large HO_2 source would be required.

Implementation of the mechanism by Fantechi et al. (2002) does not improve the model-measurement agreement of OH and HO_2 (Fig. 8) compared to the MCM. As discussed above, the mechanism by Fantechi et al. (2002) is able to describe HO_2 concentrations as well as product formation of acetone and HCHO, if pinonaldehyde is only consumed by photolysis. In

20 contrast, reaction pathways that are connected to the reaction of pinonaldehyde + OH are not correctly described.

Modeled HO_2 concentrations could be affected by the use of general reaction rate constants for reactions of RO_2 with HO_2 and NO (KRO2HO2 and KRO2NO), respectively. This might be an oversimplification for highly functionalized compounds. A sensitivity test (see Supplement) with an enhanced reaction rate for $RO_2 + NO$ reactions of $2\times$ KRO2NO in the modified mechanism by Fantechi et al. (2002) was performed. As a result, the fraction of RO_2 reacting with NO instead of HO_2 is

25 increased. This leads to an enhanced HO_2 concentration of approximately 50 % compared to the model run FAN_a. However, HO_x concentrations are again underestimated compared to measurements and the sensitivity run cannot reproduce the HO_2 concentration time behaviour from observations.

Besides reactions with NO, new types of RO_2 reactions have been recognized in the last decade that can produce HO_x. These processes include unimolecular autoxidation reactions of RO_2 (e.g. Crounse et al., 2013) and reactions of RO_2 with HO_2

30 yielding OH (e.g. Hasson et al., 2004). The new types of reactions become potentially important, when NO concentrations are below 1 ppbv. These reactions are especially favoured when the RO_2 molecule contains functional groups, like carbonyl groups as in the case of pinonaldehyde peroxy radicals. For example, acetyl- and acetonyl-RO_2 can react with HO_2 forming alkoxy radicals and OH instead of terminating the radical reaction chain forming hydroxyperoxides (Hasson et al., 2004; Dillon and Crowley, 2008). Other examples are reactions already included in the MCM, such as the photooxidation of methyl vinyl ketone

35 (Praske et al., 2015; Fuchs et al., 2018). For pinonaldehyde, there have been no comparable reactions suggested so far, although

pinonaldehyde and its degradation products have at least 2 carbonyl functions. Because 80 to 45 % of RO_2 reacts with HO_2 for conditions of the experiment here, such reaction pathways have the potential to impact the OH production rate. A sensitivity test (not shown here) shows that $RO_2 + HO_2$ reactions of RO_2 included in the mechanism with a rate of $10\times$ KRO2HO2 can reproduce measured OH concentrations. Nevertheless, the enhanced HO_2 consumption increases the model-measurement

5   discrepancy of HO_2 even more.

Reported autoxidation reactions of RO_2, which produce HO_x without NO, involve isomerization and decomposition of organic peroxy radicals. These reactions play a role, for example, in the photooxidation of isoprene (e.g. Fuchs et al., 2013; Peeters et al., 2014; Novelli et al., 2020) and methacrolein (Crounse et al., 2012; Fuchs et al., 2014), where H-shift reactions in RO_2 species lead to decomposition into a radical (OH or HO_2) and a carbonyl compound. In general, rate coefficients of

10   H-shift reactions are strongly enhanced by the presence of functional groups such as carbonyl groups, and can reach values in the order of 0.1 s^{-1} at room temperature (Crounse et al., 2013; Otkjær et al., 2018). Depending on the specific RO_2 structure and its functional groups, either OH or HO_2 can be formed. The presence of hydroxyl or hydroperoxy groups in carbonyl peroxy radicals, for example, favours the elimination of HO_2.

In the chemical degradation of pinonaldehyde to its first-generation products (Fig. 1), a large number of multifunctional

15   peroxy and alkoxy radicals are formed as intermediates. Thus, there is potential for additional HO_2 formation by unimolecular reactions. This possibility is explored in a model sensitivity run for the four oxidation branches I - IV (Fantechi et al., 2002), which follow OH addition to pinonaldehyde. The model run S1 (see Supplement) assumes that each of the initially formed peroxy radicals (C96CO3, FAN_D1, PINALO2, and FAN_G1) is eventually converted to HO_2 with a rate coefficient of 0.1 s^{-1}. However, only FAN_D1, PINALO2, and FAN_G1 have an aldehyde group with a hydrogen that can be easily abstracted (see

20   Supplementary material). The model run (Fig. 8) shows a considerable enhancement of the HO_2 concentration level in the first period of the experiment compared to model runs MCM_a and FAN_a, leading to good agreement between modeled and measured OH. However, the temporal trend of the modeled HO_2 is not well described. While the observed HO_2 shows a steady increase from the beginning to the end of the experiment, the simulation S1 shows a continuous decrease which follows the concentration of the short-lived RO_2 radicals. The opposite temporal trend suggests that additional HO_2 formation by a fast

25   process in the oxidation branches I - IV is not a likely explanation. It indicates that the additionally required HO_2 is slowly built up, probably from stable products of the pinonaldehyde oxidation.

One such possibility would be the photolysis of first-generation products. This idea is tested in model run S2 (Table 2, Fig. 8). All products of the pinonaldehyde photooxidation have either two or three carbonyl groups and therefore are likely to undergo photolysis. CO23C4CHO and C818CO even have conjugated carbonyl functions similar to glyoxal, which photolysis is up to

30   two times faster than pinonaldehyde. However, using the photolysis frequency of glyoxal as an upper limit for the photolysis frequency of the products formed here, is not sufficient to significantly improve the HO_2 model-measurement agreement. Only if a strongly enhanced photolysis frequency equivalent to $0.2 \times j_{NO2}$ is applied, modeled HO_2 comes close to the observed values. In this case, the temporal trend of the simulation is similar to the observed time behaviour of HO_2 and also OH is reasonably well reproduced. This supports the hypothesis that the additional HO_2 is slowly formed from stable oxidation

products. However, the value for the assumed photolysis frequency, which is 200 times larger than of pinonaldehyde, appears unrealistically high.

Another possibility is that the fast H-shift isomerization of RO_2 radicals (see Supplement) leads to the formation of peroxy acids with additional carbonyl functions in high yields. As discussed above, these bi-functional compounds could photolyse faster than currently implemented in the mechanism. A sensitivity test (S1_mod_hv, see Supplement) was performed that includes isomerization of RO_2 with a –HCO group. Products are assumed to photolyse with a photolysis rate that is 2 times higher than that of glyoxal. Implementation of these reactions leads to HO_2 concentrations that are increased by up to 60 % compared to the sensitivity run that includes only isomerization reactions. Calculated HO_2 concentrations underestimate measurements by factor of 2. The sensitivity test reproduces measured OH concentrations within the measurement uncertainty.

No subsequent chemistry of 4-hydroxynorpinonaldehyde is included in the mechanism so far. In the experiment here 4-hydroxynorpinonaldehyde is formed with an overall yield of approximately 25 %. 4-hydroxynorpinonaldehyde is highly functionalized and RO_2 radicals formed in its degradation could undergo fast isomerization reactions. For a sensitivity run (S3, see Supplement) a mechanism was deduced with the structure–activity relationship (SAR; Kwok and Atkinson, 1995; Vereecken and Peeters, 2009; Vereecken and Nozière, 2020) method. However, the impact of the tested 4-hydroxynorpinonaldehyde degradation scheme on the HO_2 formation was small (≤ 10 %) compared to the modified mechanism by Fantechi et al. (2002). Unfortunately, no measurements of stable oxidation products other than acetone and HCHO were available. Without further product measurements the whole analysis discussed here relies on product distribution prescribed by the models. Further experiments that measure oxidation products and yields could help to better constrain branching ratios in degradation mechanisms. In addition, theoretical studies could investigate subsequent degradation schemes of major products in more detail.

The continuous increase in the acetone and formaldehyde yields during the experiment (Fig. 5) indicates that both species are not only formed from the first reaction step of pinonaldehyde with OH, but also from further oxidation of organic products.

The base model (Fig. 3, MCM) underestimates the pinonaldehyde consumption, but shows a good model-measurement agreement with formaldehyde and acetone within the measurement uncertainty. In contrast, the model, which uses measured pinonaldehyde photolysis frequencies and is constrained to measured HO_2, produces up to 30 % less acetone and formaldehyde than measured (Fig. 5, MCM_b). The discrepancies are increasing fast during the first 2 hours of the experiment, when pinonaldehyde is the most important reaction partner for OH, and slows down, when oxidation products gain importance at later times of the experiment. The elevated HO_2 concentrations change the product distribution compared to the base case with less formed formaldehyde and acetone, because $RO_2 + HO_2$ reactions producing hydroxyperoxides become more important compared to the $RO_2 + NO$ pathway. In the chemical model, acetone and formaldehyde of this reaction pathway are formed by the slow photolysis (10 times slower than the photolysis of pinonaldehyde) of pinonic acid and perpinonic acid that are produced in the subsequent chemistry of hydroxyperoxides. Therefore, acetone and formaldehyde yields are smaller in the MCM model run, if HO_2 concentrations are correctly described compared to the base case MCM model, when HO_2 is significantly underestimated.

Implementation of the mechanism by Fantechi et al. (2002) with also HO_2 concentrations and pinonaldehyde photolysis frequency constrained to measurements (FAN_b) makes the model-measurement agreement for acetone and formaldehyde

worse. Acetone and formaldehyde yields are lowered and 4-hydroxynorpinonaldehyde and norpinonaldehyde are produced instead. Acetone and formaldehyde time series agree for the photolysis experiment, when the mechanism by Fantechi et al. (2002) is applied. Similarly, the majority of consumed pinonaldehyde (approximately 65 %) forms the peroxy radical C96O2 either by photolysis or reaction pathway I (Fig. 1), when also OH is present. Therefore, it can be assumed that the $C96O2 + NO$

5 reaction channel is not responsible for the underprediction of acetone and formaldehyde at least for the early times of the experiments, when contributions from OH reactions of product species are small. However, because $RO_2 + HO_2$ reactions are more important in the experiment with OH oxidation (see above), additional HO_2 production from this reaction pathway has the potential to serve as an explanation for the observed disccrepancies. In addition, minor pathways could produce additional formaldehyde and acetone to explain the model-measurement discrepancy right after the start of the pinonaldehyde oxidation.

10 At later times of the experiment, additional production of acetone and formaldehyde from the further degradation of oxidation products need to be assumed to close the gap. For example, this could be due to a reaction channel of the alkoxy radical $R'O8$ that does not produce norpinonaldehyde, but acetone and formaldehyde instead. However, the exact chemical mechanism that is responsible for the additional acetone and formaldehyde cannot be determined from measurements in these experiments.

Presently, there is only one work of Noziére et al. (1999) where acetone and formaldehyde were quantitatively measured for

15 the reaction of pinonaldehyde with OH. The formaldehyde yield was determined to be 1.52 ± 0.56, significantly higher than the yield measured in this work. The acetone yield in Noziére et al. (1999) lies with 0.15 ± 0.07 in the range of the acetone yield determined here for the times of the experiment when pinonaldehyde is the dominant OH reactant. In the oxidation scheme of pinonaldehyde acetone and formaldehyde are typically formed together so that similar yields would be expected. The high HCHO yield measured by Noziére et al. (1999) can be partially explained by additional fast photolysis of pinonaldehyde and

20 possibly other products by the 254 nm lamps used to generate OH by photodissociaton of H_2O_2 (Fantechi et al., 2002).

5 Summary and conclusions

The photooxidation of pinonaldehyde was investigated under natural sunlight at low NO concentrations (< 0.2 ppbv) in the presence and absence of an OH scavenger. Two experiments were conducted with maximum pinonaldehyde concentrations of 16.5 ppbv (with OH scavenger) and 6.5 ppbv (without OH scavenger). Measured times series were compared to model

25 calculations based on the recent version of the Master Chemical Mechanism (version 3.3.1).

Model results show that the pinonaldehyde consumption is underestimated in the experiment with OH scavenger. In contrast, the concentration of the measured products acetone and formaldehyde is overestimated by 60 % and 70 %, respectively. The observed decay of pinonaldehyde requires a quantum yield of 0.9 for the photolysis reaction. Previous investigations of the quantum yield determined lower yields of 0.15 (Moortgat et al., 2002) and ≤ 0.4 (Jaoui and Kamens, 2003). However, the

30 solar actinic flux could not accurately be determined in these other chamber studies and large corrections for wall loss were applied. Calculations using the measured absorption spectrum (Hallquist et al., 1997) and a quantum yield of 0.9 give photolysis frequencies, which are a factor of 3.5 times higher than values calculated by the parameterization implemented in the MCM, so that photolysis of pinonaldehyde is significantly underestimated, if this parameterization is applied.

Similarly, the pinonaldehyde consumption is underestimated by the MCM model in the experiment, where the pinonaldehyde consumption is dominated by its reaction with OH radicals. Implementing the measured photolysis frequency improves model-measurement agreement. The remaining discrepancy is caused by underestimated OH radical concentrations leading to a slower pinonaldehyde consumption. Constraining HO_2 model concentrations to the measurements brings OH concentrations in model and measurement into agreement. As a consequence, also the pinonaldehyde concentration profile is reproduced within the measurement uncertainty. The closed OH budget indicates that a HO_2 source is missing in this mechanism. The additional HO_2 source would be at least half the rate at which pinonaldehyde is consumed. HO_2 would therefore need to be reproduced much faster than current chemical models suggest in one of the major oxidation pathways. Because a large fraction of RO_2 radicals (45-80 %) react with HO_2, potential reaction pathways that do not lead to the formation of hydroxyperoxide but reform radicals have the potential to contribute the regeneration of HO_2. If fast uni-molecular RO_2 reactions existed that could compete with $RO_2 + NO$ and $RO_2 + HO_2$ reactions, they could also add to additional HO_2 production. Nevertheless, a fast degradation of first-generation products species forming HO_2 shows a better agreement with measured HO_2 concentration time profiles rather than reactions of RO_2 species.

The yield of formaldehyde in the pinonaldehyde photolysis with OH scavenger present is determined to be 0.18 ± 0.20. No acetone formation is observed. Model calculations based on the MCM constrained with the measured photolysis frequency overestimate formaldehyde and acetone concentrations by a factor of approximately 3. In the experiment with OH the yields of acetone and formaldehyde increase over the course of the experiment from (0.2 ± 0.1) to (0.3 ± 0.1) and from (0.15 ± 0.2) to (0.45 ± 0.2) respectively. The increasing yields indicate that both species are also formed by the subsequent chemistry of products formed in the first reaction steps.

Modifications of the degradation mechanism proposed by Fantechi et al. (2002), including a new product distribution and additional products for the initial attack of OH, reproduce measured acetone and formaldehyde concentrations within their uncertainty as long as the reaction with OH is supressed. In the experiment with OH, the model-measurement agreement for both species decrease after implementing the modifications by Fantechi et al. (2002). This indicates that the pathways relevant when OH is dominating the fate of pinonaldehyde lack sources of acetone and formaldehyde in this case.

Field campaigns in environments dominated by monoterpene emissions like the Bio-hydro-atmosphere interactions of Energy, Aerosols, Carbon, H2O, Organics, and Nitrogen–Rocky Mountain Organic Carbon Study (BEACHON-ROCS; Kim et al., 2013) or the Hyytiälä United Measurements of Photochemistry and Particles in Air — Comprehensive Organic Precursor Emission and Concentration study (HUMPPA-COPEC; Hens et al., 2014) showed that OH and HO_2 radical concentrations were underestimated in model calculations by up to a factor of 2.5. Constraining modeled HO_2 concentrations to measurements allowed reproducing OH radical concentrations. In addition, also chamber studies on the photooxidation of α-pinene (Rolletter et al., 2019) and β-pinene (Kaminski et al., 2017) confirmed that the current α and β-pinene mechanisms lack HO_2 sources. It is currently unknown, if the missing source is part of reactions forming first generation products or of the subsequent chemistry of the degradation products. Here, it is shown that also in the mechanism of the photoxodidation of pinonaldehyde, a degradation product of α-pinene, a HO_2 source is missing. However, the findings here cannot explain the discrepancies observed in the α-pinene chamber experiments and field campaigns, because the pinonaldehyde yield in the α-pinene degradation is

rather small (5 %, Rolletter et al. (2019)). Nevertheless, this result is an example for a second-generation species that produces significantly more HO_2 than suggested in current chemical models. Further experiments will be required to investigate, if also other oxidation products from the degradation of monoterpenes could explain observations of missing HO_2 sources.

Data availability. Data of the experiments in the SAPHIR chamber used in this work is available on the EUROCHAMP data homepage

5 (https://data.eurochamp.org/) (Eurochamp, 2019).

Author contributions. MR analysed the data and wrote the paper. HF and MK designed the experiments. HF conducted the HO_x radical measurements. BB conducted the radiation measurements. MK and RW were responsible for the GC measurements. RT was responsible for the PTR-TOF-MS measurements. XL was responsible for the HONO measurements and HPD for the DOAS OH data. FR was responsible for the NO_x and O_3 data. All co-authors commented on the manuscript.

10 *Competing interests.* The authors declare to have no competing interests.

Acknowledgements. This work was supported by the EU Horizon 2020 program Eurochamp2020 (grant agreement no. 730997). This project has received funding from the European Research Council (ERC) under the European Union's Horizon 2020 research and innovation programme (SARLEP grant agreement No. 681529) The authors thank Luc Vereecken for his help with the 4-hydroxynorpinonaldehyde mechanism.

References

Alves, C., Carvalho, A., and Pio, C.: Mass balance of organic carbon fractions in atmospheric aerosols, J. Geophys. Res. Atmos., 107, ICC 7–1–ICC 7–9, https://doi.org/10.1029/2001jd000616, 2002.

Atkinson, R. and Arey, J.: Atmospheric degradation of volatile organic compounds, Chem. Rev., 103, 4605–4638, https://doi.org/10.1021/cr0206420, 2003.

Atkinson, R., Baulch, D. L., Cox, R. A., Crowley, J. N., Hampson, R. F., Hynes, R. G., Jenkin, M. E., Rossi, M. J., and Troe, J.: Evaluated kinetic and photochemical data for atmospheric chemistry: Volume I - gas phase reactions of O_x, HO_x, NO_x and SO_x species, Atmos. Chem. Phys., 4, 1461–1738, https://doi.org/10.5194/acp-4-1461-2004, 2004.

Atkinson, R., Baulch, D. L., Cox, R. A., Crowley, J. N., Hampson, R. F., Hynes, R. G., Jenkin, M. E., Rossi, M. J., Troe, J., and Subcommittee, I.: Evaluated kinetic and photochemical data for atmospheric chemistry: Volume II - gas phase reactions of organic species, Atmos. Chem. Phys., 6, 3625–4055, https://doi.org/10.5194/acp-6-3625-2006, 2006.

Bohn, B. and Zilken, H.: Model-aided radiometric determination of photolysis frequencies in a sunlit atmosphere simulation chamber, Atmos. Chem. Phys., 5, 191–206, https://doi.org/10.5194/acp-5-191-2005, 2005.

Bohn, B., Rohrer, F., Brauers, T., and Wahner, A.: Actinometric measurements of NO_2 photolysis frequencies in the atmosphere simulation chamber SAPHIR, Atmos. Chem. Phys., 5, 493–503, https://doi.org/10.5194/acp-5-493-2005, 2005.

Boy, M., Petäjä, T., Dal Maso, M., Rannik, U., Rinne, J., Aalto, P., Laaksonen, A., Vaattovaara, P., Joutsensaari, J., Hoffmann, T., Warnke, J., Apostolaki, M., Stephanou, E. G., Tsapakis, M., Kouvarakis, A., Pio, C., Carvalho, A., Römpp, A., Moortgat, G., Spirig, C., Guenther, A., Greenberg, J., Ciccioli, P., and Kulmala, M.: Overview of the field measurement campaign in Hyytiälä, August 2001 in the framework of the EU project OSOA, Atmos. Chem. Phys., 4, 657–678, https://doi.org/10.5194/acp-4-657-2004, 2004.

Cahill, T. M., Seaman, V. Y., Charles, M. J., Holzinger, R., and Goldstein, A. H.: Secondary organic aerosols formed from oxidation of biogenic volatile organic compounds in the Sierra Nevada Mountains of California, J. Geophys. Res. Atmos., 111, 14, https://doi.org/10.1029/2006jd007178, 2006.

Calogirou, A., Larsen, B. R., and Kotzias, D.: Gas-phase terpene oxidation products: a review, Atmos. Environ., 33, 1423–1439, https://doi.org/10.1016/S1352-2310(98)00277-5, 1999.

Capouet, M., Peeters, J., Noziére, B., and Müller, J. F.: Alpha-pinene oxidation by OH: simulations of laboratory experiments, Atmos. Chem. Phys., 4, 2285–2311, https://doi.org/10.5194/acp-4-2285-2004, 2004.

Crounse, J. D., Knap, H. C., Ornso, K. B., Jorgensen, S., Paulot, F., Kjaergaard, H. G., and Wennberg, P. O.: On the atmospheric fate of methacrolein: 1. Peroxy radical isomerization following addition of OH and O_2, J. Phys. Chem. A, 116, 5756–5762, https://doi.org/10.1021/jp211560u, 2012.

Crounse, J. D., Nielsen, L. B., Jørgensen, S., Kjaergaard, H. G., and Wennberg, P. O.: Autoxidation of organic compounds in the atmosphere, J. Phys. Chem. Lett., 4, 3513–3520, https://doi.org/10.1021/jz4019207, 2013.

Dash, M. R. and Rajakumar, B.: Abstraction kinetics of H-atom by OH radical from pinonaldehyde ($C_{10}H_{16}O_2$): Ab initio and transition-state theory Calculations, J. Phys. Chem. A, 116, 5856–5866, https://doi.org/10.1021/jp209208e, 2012.

Daumont, D., Brion, J., Charbonnier, J., and Malicet, J.: Ozone UV spectroscopy I: Absorption cross-sections at room temperature, J. Atmos. Chem., 15, 145–155, https://doi.org/10.1007/bf00053756, 1992.

Dillon, T. J. and Crowley, J. N.: Direct detection of OH formation in the reactions of HO_2 with $CH_3C(O)O_2$ and other substituted peroxy radicals, Atmos. Chem. Phys., 8, 4877–4889, https://doi.org/10.5194/acp-8-4877-2008, 2008.

Dorn, H.-P., Brandenburger, U., Brauers, T., and Hausmann, M.: A new in-situ laser long-path absorption instrument for the measurement of tropospheric OH radicals, J. Atmos. Sci., 52, 3373–3380, 1995a.

Dorn, H. P., Neuroth, R., and Hofzumahaus, A.: Investigation of OH absorption cross sections of rotational transitions in the $A^2\Sigma^+$, $\nu' = 0 \leftarrow X^2\Pi$, $\nu'' = 0$ band under atmospheric conditions: Implications for tropospheric long-path absorption measurements, J. Geophys. Res., 100, 7397–7409, https://doi.org/10.1029/94jd03323, 1995b.

Eurochamp: Database of Atmospheric Simulation Chamber Studies, https://data.eurochamp.org/, last access: 9 September, 2019.

Fantechi, G., Vereecken, L., and Peeters, J.: The OH-initiated atmospheric oxidation of pinonaldehyde: Detailed theoretical study and mechanism construction, Phys. Chem. Chem. Phys., 4, 5795–5805, https://doi.org/10.1039/B205901K, 2002.

Fuchs, H., Bohn, B., Hofzumahaus, A., Holland, F., Lu, K. D., Nehr, S., Rohrer, F., and Wahner, A.: Detection of HO_2 by laser-induced fluorescence: calibration and interferences from RO_2 radicals, Atmos. Meas. Tech., 4, 1209–1255, https://doi.org/10.5194/amt-4-1209-2011, 2011.

Fuchs, H., Dorn, H. P., Bachner, M., Bohn, B., Brauers, T., Gomm, S., Hofzumahaus, A., Holland, F., Nehr, S., Rohrer, F., Tillmann, R., and Wahner, A.: Comparison of OH concentration measurements by DOAS and LIF during SAPHIR chamber experiments at high OH reactivity and low NO concentration, Atmos. Meas. Tech., 5, 1611–1626, https://doi.org/10.5194/amt-5-1611-2012, 2012.

Fuchs, H., Hofzumahaus, A., Rohrer, F., Bohn, B., Brauers, T., Dorn, H.-P., Häseler, R., Holland, F., Kaminski, M., Li, X., Lu, K., Nehr, S., Tillmann, R., Wegener, R., and Wahner, A.: Experimental evidence for efficient hydroxyl radical regeneration in isoprene oxidation, Nat. Geosci., 6, 1023–1026, https://doi.org/10.1038/NGEO1964, 2013.

Fuchs, H., Acir, I. H., Bohn, B., Brauers, T., Dorn, H. P., Häseler, R., Hofzumahaus, A., Holland, F., Kaminski, M., Li, X., Lu, K., Lutz, A., Nehr, S., Rohrer, F., Tillmann, R., Wegener, R., and Wahner, A.: OH regeneration from methacrolein oxidation investigated in the atmosphere simulation chamber SAPHIR, Atmos. Chem. Phys., 14, 7895–7908, https://doi.org/10.5194/acp-14-7895-2014, 2014.

Fuchs, H., Albrecht, S., Acir, I. H., Bohn, B., Breitenlechner, M., Dorn, H. P., Gkatzelis, G. I., Hofzumahaus, A., Holland, F., Kaminski, M., Keutsch, F. N., Novelli, A., Reimer, D., Rohrer, F., Tillmann, R., Vereecken, L., Wegener, R., Zaytsev, A., Kiendler-Scharr, A., and Wahner, A.: Investigation of the oxidation of methyl vinyl ketone (MVK) by OH radicals in the atmospheric simulation chamber SAPHIR, Atmos. Chem. Phys., 2018, 8001–8016, https://doi.org/10.5194/acp-18-8001-2018, 2018.

Galloway, M. M., Huisman, A. J., Yee, L. D., Chan, A. W. H., Loza, C. L., Seinfeld, J. H., and Keutsch, F. N.: Yields of oxidized volatile organic compounds during the OH radical initiated oxidation of isoprene, methyl vinyl ketone, and methacrolein under high-NO_X conditions, Atmos. Chem. Phys., 11, 10779–10790, https://doi.org/10.5194/acp-11-10779-2011, 2011.

Glasius, M., Calogirou, A., Jensen, J., Hjorth, J., and Nielsen, C. J.: Kinetic study of gas-phase reactions of pinonaldehyde and structurally related compounds, Int. J. Chem. Kin., 29, 527–533, https://doi.org/10.1002/(sici)1097-4601(1997)29:7<527::Aid-kin7>3.0.Co;2-w, 1997.

Guenther, A. B., Jiang, X., Heald, C. L., Sakulyanontvittaya, T., Duhl, T., Emmons, L. K., and Wang, X.: The model of emissions of gases and aerosols from nature version 2.1 (MEGAN2.1): an extended and updated framework for modeling biogenic emissions, Geosci. Model Dev., 5, 1471–1492, https://doi.org/10.5194/gmd-5-1471-2012, 2012.

Hallquist, M., Wängberg, I., and Ljungström, E.: Atmospheric fate of carbonyl oxidation products originating from α-pinene and Δ^3-carene: determination of rate of reaction with OH and NO_3 radicals, UV absorption cross sections, and vapor pressures, Environ. Sci. Technol., 31, 3166–3172, https://doi.org/10.1021/es970151a, 1997.

Hasson, A. S., Tyndall, G. S., and Orlando, J. J.: A product yield study of the reaction of HO_2 radicals with ethyl peroxy ($C_2H_5O_2$), acetyl peroxy ($CH_3C(O)O_2$), and acetonyl peroxy ($CH_3C(O)CH_2O_2$) radicals, J. Phys. Chem. A, 108, 5979–5989, https://doi.org/10.1021/jp048873t, 2004.

Hausmann, M., Brandenburger, U., Brauers, T., and Dorn, H.-P.: Detection of tropospheric OH radicals by long-path differential-optical-absorption spectroscopy: Experimental setup, accuracy, and precision, J. Geophys. Res., 102, 16 011–16 022, https://doi.org/10.1029/97jd00931, 1997.

Hens, K., Novelli, A., Martinez, M., Auld, J., Axinte, R., Bohn, B., Fischer, H., Keronen, P., Kubistin, D., Nölscher, A. C., Oswald, R., Paaso-nen, P., Petäjä, T., Regelin, E., Sander, R., Sinha, V., Sipilä, M., Taraborrelli, D., Tatum Ernest, C., Williams, J., Lelieveld, J., and Harder, H.: Observation and modelling of HO_X radicals in a boreal forest, Atmos. Chem. Phys., 14, 8723–8747, https://doi.org/10.5194/acp-14-8723-2014, 2014.

Herckes, P., Engling, G., Kreidenweis, S. M., and Collett, J. L.: Particle size distributions of organic aerosol constituents during the 2002 Yosemite Aerosol Characterization Study, Environ. Sci. Technol., 40, 4554–4562, https://doi.org/10.1021/es0515396, 2006.

Hofzumahaus, A.: Measurement of Photolysis Frequencies in the Atmosphere, in: Analytical Techniques for Atmospheric Measurement, D.E. Heard (Ed.), book section 9, pp. 406–500, https://doi.org/10.1002/9780470988510.ch9, 2006.

Holland, F., Hofzumahaus, A., Schäfer, J., Kraus, A., and Pätz, H. W.: Measurements of OH and HO_2 radical concentrations and photolysis frequencies during BERLIOZ, J. Geophys. Res., 108, 8246, https://doi.org/10.1029/2001JD001393, 2003.

Jacob, D. J., Field, B. D., Jin, E. M., Bey, I., Li, Q., Logan, J. A., and Yantosca, R. M.: Atmospheric acetone budget, J. Geophys. Res., 107, 4100, https://doi.org/10.1029/2001JD000694, 2002.

Jaoui, M. and Kamens, R. M.: Gas phase photolysis of pinonaldehyde in the presence of sunlight, Atmos. Environ., 37, 1835–1851, https://doi.org/10.1016/S1352-2310(03)00033-5, 2003.

Jenkin, M. E., Saunders, S. M., and Pilling, M. J.: The tropospheric degradation of volatile organic compounds: A protocol for mechanism development, Atmos. Environ., 31, 81–104, https://doi.org/10.1016/S1352-2310(96)00105-7, 1997.

Jordan, A., Haidacher, S., Hanel, G., Hartungen, E., Märk, L., Seehauser, H., Schottkowsky, R., Sulzer, P., and Märk, T. D.: A high resolution and high sensitivity proton-transfer-reaction time-of-flight mass spectrometer (PTR-TOF-MS), Int. J. Mass Spectrom., 286, 122–128, https://doi.org/10.1016/j.ijms.2009.07.005, 2009.

Kaminski, M., Fuchs, H., Acir, I. H., Bohn, B., Brauers, T., Dorn, H. P., Häseler, R., Hofzumahaus, A., Li, X., Lutz, A., Nehr, S., Rohrer, F., Tillmann, R., Vereecken, L., Wegener, R., and Wahner, A.: Investigation of the β-pinene photooxidation by OH in the atmosphere simulation chamber SAPHIR, Atmos. Chem. Phys., 17, 6631–6650, https://doi.org/10.5194/acp-17-6631-2017, 2017.

Kanakidou, M., Tsigaridis, K., Dentener, F. J., and Crutzen, P. J.: Human-activity-enhanced formation of organic aerosols by biogenic hydrocarbon oxidation, J. Geophys. Res., 105, 9243–9354, https://doi.org/10.1029/1999JD901148, 2000.

Karl, M., Dorn, H.-P., Holland, F., Koppmann, R., Poppe, D., Rupp, L., Schaub, A., and Wahner, A.: Product study of the reaction of OH radicals with isoprene in the atmosphere simulation chamber SAPHIR, J. Atmos. Chem., 55, 167–187, https://doi.org/10.1007/s10874-006-9034-x, 2006.

Kavouras, I. G., Mihalopoulos, N., and Stephanou, E. G.: Formation and gas/particle partitioning of monoterpenes photo-oxidation products over forests, Geophys. Res. Lett., 26, 55–58, https://doi.org/10.1029/1998gl900251, 1999.

Kim, S., Wolfe, G. M., Mauldin, L., Cantrell, C., Guenther, A., Karl, T., Turnipseed, A., Greenberg, J., Hall, S. R., Ullmann, K., Apel, E., Hornbrook, R., Kajii, Y., Nakashima, Y., Keutsch, F. N., DiGangi, J. P., Henry, S. B., Kaser, L., Schnitzhofer, R., Graus, M., and Hansel, A.: Evaluation of HO_X sources and cycling using measurement-constrained model calculations in a 2-methyl-3-butene-2-ol (MBO) and monoterpene (MT) dominated ecosystem, Atmos. Chem. Phys., 13, 2031–2044, https://doi.org/10.5194/acp-13-2031-2013, 2013.

Kwok, E. S. C. and Atkinson, R.: Estimation of hydroxyl radical reaction rate constants for gas-phase organic compounds using a structure-reactivity relationship: An update, Atmos. Environ., 29, 1685–1695, https://doi.org/10.1016/1352-2310(95)00069-B, 1995.

Larsen, B. R., Di Bella, D., Glasius, M., Winterhalter, R., Jensen, N. R., and Hjorth, J.: Gas-phase OH oxidation of monoterpenes: Gaseous and particulate products, J. Atmos. Chem., 38, 231–276, https://doi.org/10.1023/A:1006487530903, 2001.

Lew, M. M., Dusanter, S., and Stevens, P. S.: Measurement of interferences associated with the detection of the hydroperoxy radical in the atmosphere using laser-induced fluorescence, Atmos. Meas. Tech., 11, 95–108, https://doi.org/10.5194/amt-11-95-2018, 2018.

5 Li, X., Rohrer, F., Hofzumahaus, A., Brauers, T., Häseler, R., Bohn, B., Broch, S., Fuchs, H., Gomm, S., Holland, F., Jäger, J., Kaiser, J., Keutsch, F. N., Lohse, I., Lu, K., Tillmann, R., Wegener, R., Wolfe, G. M., Mentel, T. F., Kiendler-Scharr, A., and Wahner, A.: Missing gas-phase source of HONO inferred from Zeppelin measurements in the troposphere, Science, 344, 292–296, https://doi.org/10.1126/science.1248999, 2014.

Lindinger, W., Hansel, A., and Jordan, A.: On-line monitoring of volatile organic compounds at pptv levels by means of proton-transfer-
10 reaction mass spectrometry (PTR-MS) - Medical applications, food control and environmental research, Int. J. Mass Spectrom., 173, 191–241, https://doi.org/10.1016/s0168-1176(97)00281-4, 1998.

Martinez, R. D., Buitrago, A. A., Howell, N. W., Hearn, C. H., and Joens, J. A.: The near U.V. absorption spectra of several aliphatic aldehydes and ketones at 300 K, Atmos. Environ., 26, 785–792, https://doi.org/10.1016/0960-1686(92)90238-G, 1992.

Matsumi, Y., Comes, F. J., Hancock, G., Hofzumahaus, A., Hynes, A. J., Kawasaki, M., and Ravishankara, A. R.: Quantum yields for
15 production of O(^{1}D) in the ultraviolet photolysis of ozone: Recommendation based on evaluation of laboratory data, J. Geophys. Res. Atmos., 107, ACH 1–1–ACH 1–12, https://doi.org/10.1029/2001jd000510, 2002.

MCM: Master Chemical Mechanism, http://mcm.leeds.ac.uk/MCM/, last access: 04 March 2020, 2017.

Mérienne, M. F., Jenouvrier, A., and Coquart, B.: The NO_2 absorption spectrum. I: Absorption cross-sections at ambient temperature in the 300-500 nm region, J. Atmos. Chem., 20, 281–297, https://doi.org/10.1007/bf00694498, 1995.

20 Moortgat, G., Wirtz, K., Hjorth, J., Ljungstrom, E., Ruppert, L., Hayman, G., and Mellouki, W.: 'Evaluation of radical sources in atmospheric chemistry through chamber and laboratory studies', Final report on the EU project 'RADICAL', Report EUR 20254 EN., 2002.

Müller, K., Haferkorn, S., Grabmer, W., Wisthaler, A., Hansel, A., Kreuzwieser, J., Cojocariu, C., Rennenberg, H., and Herrmann, H.: Biogenic carbonyl compounds within and above a coniferous forest in Germany, Atmos. Environ., 40, 81–91, https://doi.org/10.1016/j.atmosenv.2005.10.070, 2006.

25 Novelli, A., Vereecken, L., Bohn, B., Dorn, H. P., Gkatzelis, G. I., Hofzumahaus, A., Holland, F., Reimer, D., Rohrer, F., Rosanka, S., Taraborrelli, D., Tillmann, R., Wegener, R., Yu, Z., Kiendler-Scharr, A., Wahner, A., and Fuchs, H.: Importance of isomerization reactions for OH radical regeneration from the photo-oxidation of isoprene investigated in the atmospheric simulation chamber SAPHIR, Atmos. Chem. Phys., 20, 3333–3355, https://doi.org/10.5194/acp-20-3333-2020, 2020.

Noziére, B., Barnes, I., and Becker, K.-H.: Product study and mechanisms of the reactions of α-pinene and of pinonaldehyde with OH
30 radicals, J. Geophys. Res., 104, 23 645–23 656, https://doi.org/10.1029/1999JD900778, 1999.

Otkjær, R. V., Jakobsen, H. H., Tram, C. M., and Kjaergaard, H. G.: Calculated Hydrogen Shift Rate Constants in Substituted Alkyl Peroxy Radicals, J. Phys. Chem. A,, 122, 8665–8673, https://doi.org/10.1021/acs.jpca.8b06223, 2018.

Peeters, J., Vereecken, L., and Fantechi, G.: The detailed mechanism of the OH-initiated atmospheric oxidation of α-pinene: a theoretical study, Phys. Chem. Chem. Phys., 3, 5489–5504, https://doi.org/10.1039/B106555F, 2001.

35 Peeters, J., Müller, J.-F., Stavrakou, T., and Nguyen, V. S.: Hydroxyl radical recycling in isoprene oxidation driven by hydrogen bonding and hydrogen tunneling: The upgraded LIM1 mechanism, J. Phys. Chem. A, 118, 8625–8643, https://doi.org/10.1021/jp5033146, 2014.

Plewka, A., Gnauk, T., Bruggemann, E., and Herrmann, H.: Biogenic contributions to the chemical composition of airborne particles in a coniferous forest in Germany, Atmos. Environ., 40, S103–S115, https://doi.org/10.1016/j.atmosenv.2005.09.090, 2006.

Praske, E., Crounse, J. D., Bates, K. H., Kurten, T., Kjaergaard, H. G., and Wennberg, P. O.: Atmospheric fate of methyl vinyl ketone: Peroxy radical reactions with NO and HO_2, J. Phys. Chem. A, 119, 4562–4572, https://doi.org/10.1021/jp5107058, 2015.

Rissanen, T., Hyotylainen, T., Kallio, M., Kronholm, J., Kulmala, M., and Rikkola, M. L.: Characterization of organic compounds in aerosol particles from a coniferous forest by GC-MS, Chemosphere, 64, 1185–1195, https://doi.org/10.1016/j.chemosphere.2005.11.079, 2006.

5   Rohrer, F. and Brüning, D.: Surface NO and NO_2 mixing ratios measured between $30°N$ and $30°S$ in the Atlantic region, J. Atmos. Chem., 15, 253–267, https://doi.org/10.1029/97JD01853, 1992.

Rohrer, F., Bohn, B., Brauers, T., Brüning, D., Johnen, F.-J., Wahner, A., and Kleffmann, J.: Characterisation of the photolytic HONO-source in the atmosphere simulation chamber SAPHIR, Atmos. Chem. Phys., 5, 2189–2201, https://doi.org/10.5194/acp-5-2189-2005, 2005.

Rolletter, M., Kaminski, M., Acir, I. H., Bohn, B., Dorn, H. P., Li, X., Lutz, A., Nehr, S., Rohrer, F., Tillmann, R., Wegener, R., Hofzumahaus,
10   A., Kiendler-Scharr, A., Wahner, A., and Fuchs, H.: Investigation of the α-pinene photooxidation by OH in the atmospheric simulation chamber SAPHIR, Atmos. Chem. Phys., 19, 11 635–11 649, https://doi.org/10.5194/acp-19-11635-2019, 2019.

Satsumabayashi, H., Nishizawa, H., Yokouchi, Y., and Ueda, H.: Pinonaldehyde and some other organics in rain and snow in central Japan, Chemosphere, 45, 887–891, https://doi.org/10.1016/s0045-6535(01)00024-8, 2001.

Saunders, S. M., Jenkin, M. E., Derwent, R. G., and Pilling, M. J.: Protocol for the development of the Master Chemical Mecha-
15   nism, MCMv3 (Part A): Tropospheric degradation of non-aromatic volatile organic compounds, Atmos. Chem. Phys., 3, 161–180, https://doi.org/10.5194/acp-3-161-2003, 2003.

Schlosser, E., Bohn, B., Brauers, T., Dorn, H.-P., Fuchs, H., Häseler, R., Hofzumahaus, A., Holland, F., Rohrer, F., Rupp, L. O., Siese, M., Tillmann, R., and Wahner, A.: Intercomparison of two hydroxyl radical measurement techniques at the atmosphere simulation chamber SAPHIR, J. Atmos. Chem., 56, 187–205, https://doi.org/10.1007/s10874-006-9049-3, 2007.

20   Schwantes, R. H., Emmons, L. K., Orlando, J. J., Barth, M. C., Tyndall, G. S., Hall, S. R., Ullmann, K., St. Clair, J. M., Blake, D. R., Wisthaler, A., and Bui, T. P. V.: Comprehensive isoprene and terpene gas-phase chemistry improves simulated surface ozone in the southeastern US, Atmos. Chem. Phys., 20, 3739–3776, https://doi.org/10.5194/acp-20-3739-2020, 2020.

Stutz, J., Kim, E. S., Platt, U., Bruno, P., Perrino, C., and Febo, A.: UV-visible absorption cross sections of nitrous acid, J. Geophys. Res. Atmos., 105, 14 585–14 592, https://doi.org/10.1029/2000jd900003, 2000.

25   Tadić, J., Juranić, I., and Moortgat, G. K.: Pressure dependence of the photooxidation of selected carbonyl compounds in air: n-butanal and n-pentanal, J. Photochem. Photobiol. A, 143, 169–179, https://doi.org/https://doi.org/10.1016/S1010-6030(01)00524-X, 2001.

Troe, J.: Are primary quantum yields of NO2 photolysis at $\lambda \leq 398$ nm smaller than unity?, Z. Phys. Chem., 214, 573, https://doi.org/10.1524/zpch.2000.214.5.573, 2000.

Vereecken, L. and Nozière, B.: H migration in peroxy radicals under atmospheric conditions, Atmos. Chem. Phys., 20, 7429–7458,
30   https://doi.org/10.5194/acp-20-7429-2020, 2020.

Vereecken, L. and Peeters, J.: Enhanced H-atom abstraction from pinonaldehyde, pinonic acid, pinic acid, and related compounds: theoretical study of C-H bond strengths, Phys. Chem. Chem. Phys., 4, 467–472, https://doi.org/10.1039/B109370C, 2002.

Vereecken, L. and Peeters, J.: Decomposition of substituted alkoxy radicals-part I: a generalized structure-activity relationship for reaction barrier heights, Phys. Chem. Chem. Phys., 11, 9062–9074, https://doi.org/10.1039/B909712K, 2009.

35   Vereecken, L., Müller, J. F., and Peeters, J.: Low-volatility poly-oxygenates in the OH-initiated atmospheric oxidation of α-pinene: impact of non-traditional peroxyl radical chemistry, Phys. Chem. Chem. Phys., 9, 5241–5248, https://doi.org/10.1039/B708023A, 2007.

Whalley, L. K., Blitz, M. A., Desservettaz, M., Seakins, P. W., and Heard, D. E.: Reporting the sensitivity of laser-induced fluorescence instruments used for HO_2 detection to an interference from RO_2 radicals and introducing a novel approach that enables HO_2 and certain RO_2 types to be selectively measured, Atmos. Meas. Tech., 6, 3425–3440, https://doi.org/10.5194/amt-6-3425-2013, 2013.

Xu, L., Møller, K. H., Crounse, J. D., Otkjær, R. V., Kjaergaard, H. G., and Wennberg, P. O.: Unimolecular Reactions of Peroxy Radicals Formed in the Oxidation of α-Pinene and β-Pinene by Hydroxyl Radicals, J. Phys. Chem. A,, 123, 1661–1674, https://doi.org/10.1021/acs.jpca.8b11726, 2019.

Yu, J. Z., Griffin, R. J., Cocker, D. R., Flagan, R. C., Seinfeld, J. H., and Blanchard, P.: Observation of gaseous and particulate products of monoterpene oxidation in forest atmospheres, Geophys. Res. Lett., 26, 1145–1148, https://doi.org/10.1029/1999gl900169, 1999.

Table 1. Instrumentation for radical and trace gas detection during the pinonaldehyde oxidation experiments.

	Technique	Time Resolution	1σ Precision	1σ Accuracy
OH	DOAS[a] (Dorn et al., 1995a; Hausmann et al., 1997; Schlosser et al., 2007)	205 s	0.8×10^6 cm^{-3}	6.5 %
OH	LIF[b] (Holland et al., 2003; Fuchs et al., 2012)	47 s	0.3×10^6 cm^{-3}	13 %
HO$_2$	LIF[b] (Fuchs et al., 2011)	47 s	1.5×10^7 cm^{-3}	16 %
NO	Chemiluminescence (Rohrer and Brüning, 1992)	180 s	4 pptv	5 %
NO$_2$	Chemiluminescence (Rohrer and Brüning, 1992)	180 s	2 pptv	5 %
O$_3$	UV absorption (Ansyco)	10 s	5 ppbv	5 %
pinonaldehyde, acetone	PTR-TOF-MS[c] (Lindinger et al., 1998)	30 s	15 pptv	6 %
acetone	GC-FID[d] (Kaminski et al., 2017)	30 min	20 pptv	5 %
HCHO	Hantzsch monitor (AeroLaser)	120 s	20 pptv	5 %
HCHO	DOAS[a]	100 s	20 %	10 %
HONO	LOPAP[e] (Li et al., 2014)	300 s	1.3 pptv	13 %
Photolysis frequencies	Spectroradiometer (Bohn et al., 2005)	60 s	10 %	10 %

[a] Differential Optical Absorption Spectroscopy

[b] Laser Induced Fluorescence

[c] Proton-Transfer-Reaction Time-Of-Flight Mass-Spectrometry

[d] Gas Chromatography Flame-Ionization-Detector

[e] Long-Path-Absorption-Photometer

Table 2. Overview of different model calculations.

Model run	Model	$j_{\text{pinonaldehyde}}$	HO_2
MCM	MCM[a]	MCM[b]	calculated
MCM_a	MCM[a]	exp.[c]	calculated
MCM_b	MCM[a]	exp.[c]	constrained
FAN_a	Fantechi et al.[d]	exp.[c]	calculated
FAN_b	Fantechi et al.[d]	exp.[c]	constrained
S1	like FAN_a, with additional $RO_2 \rightarrow HO_2$ ($0.1\,\text{s}^{-1}$)		
	for RO_2 = C96CO3, FAN_D1, PINALO2, and FAN_G1		
S2	like FAN_a, with additional photolysis ($0.2 \times j_{\text{NO2}}$)		
	of first generation pinonaldehyde products		
	(4-hydroxynorpinonaldehyde, NORPINAL,		
	CO13C4CHO, CO23C4CHO, C818CO)		

[a]Master Chemical Mechanism v3.3.1

[b]Parametrization used by MCM v3.3.1

[c]Calculated from the measured solar actinic spectrum, using the absorption spectrum by Hallquist et al. (1997) and an estimated effective quantum yield of 0.9

[d]Mechanism by Fantechi et al. (2002) replaces pinonaldehyde chemistry in MCM (see Supplement)
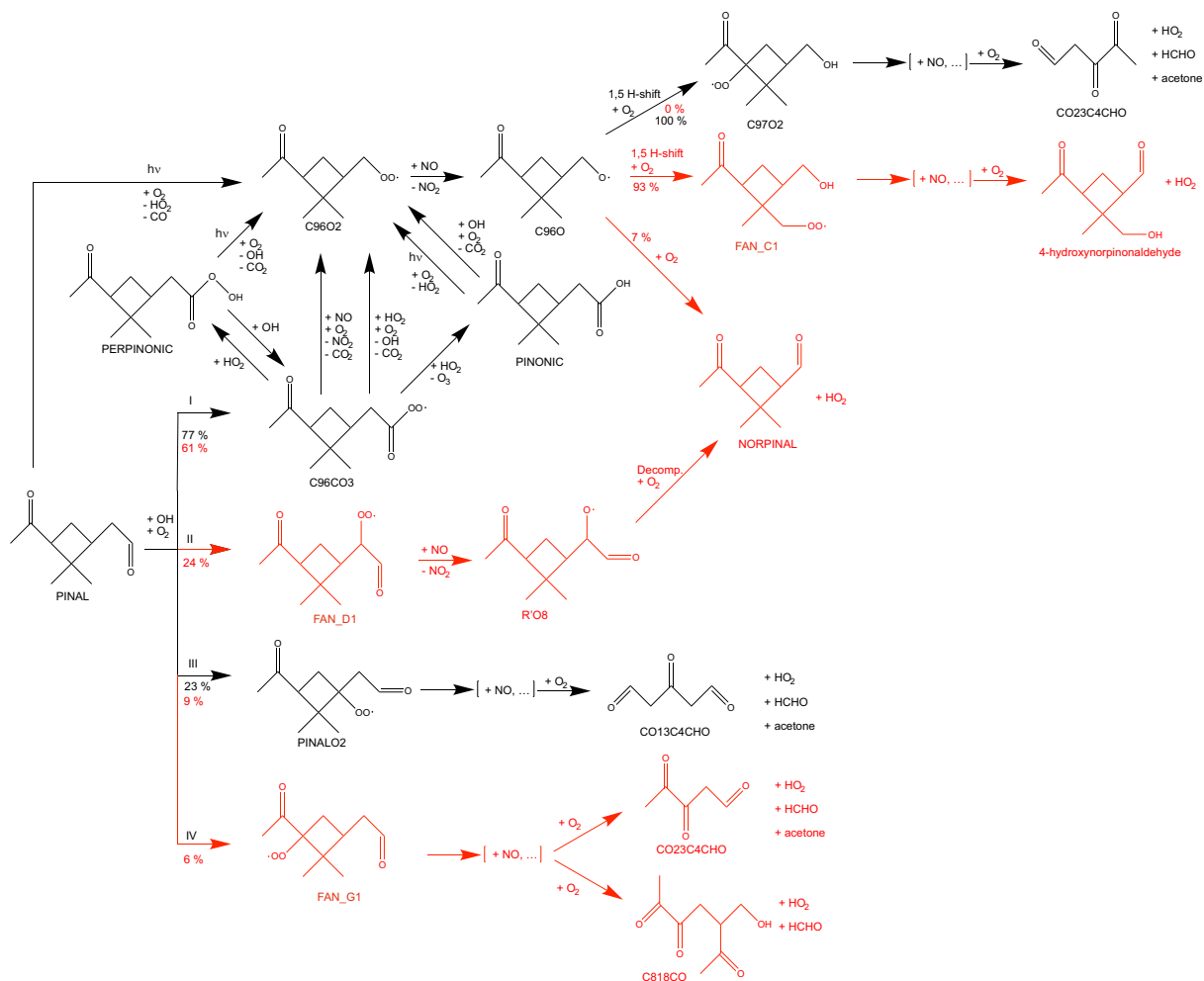
Figure 1. Simplified oxidation scheme of pinonaldehyde as described in the MCM (black) and modifications in the model derived by Fantechi et al. (2002) shown in red. [+NO, ...] represents reaction sequences which are initiated by peroxy radical reactions with NO and eventually form carbonyl compounds plus HO_2. Possible reactions of RO_2 with other RO_2 are not shown. $RO_2 + HO_2$ reactions are only shown for the major peroxy radical C96CO3. See text for details.
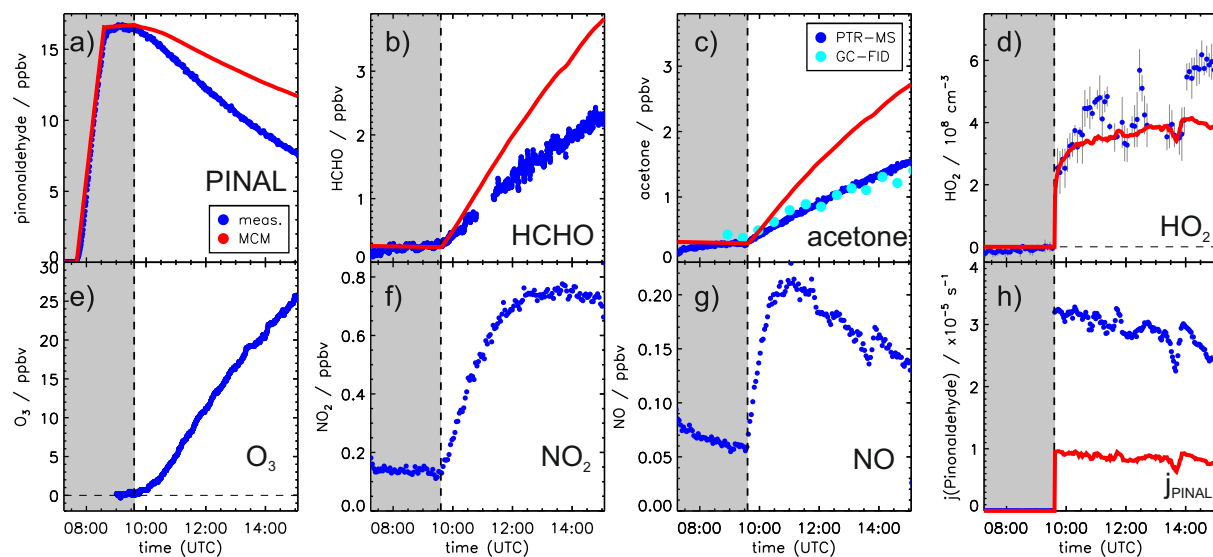
Figure 2. Measured and modeled trace gas concentrations and photolysis frequencies during photooxidation of pinonaldehyde in the presence of an OH scavenger. Pinonaldehyde is removed by photolysis, only. Measured O_3, NO_2 and NO were used as constraints for the model. See text for details of the pinonaldehyde photolysis frequency (h). Grey shaded areas indicate times when the chamber roof was closed.
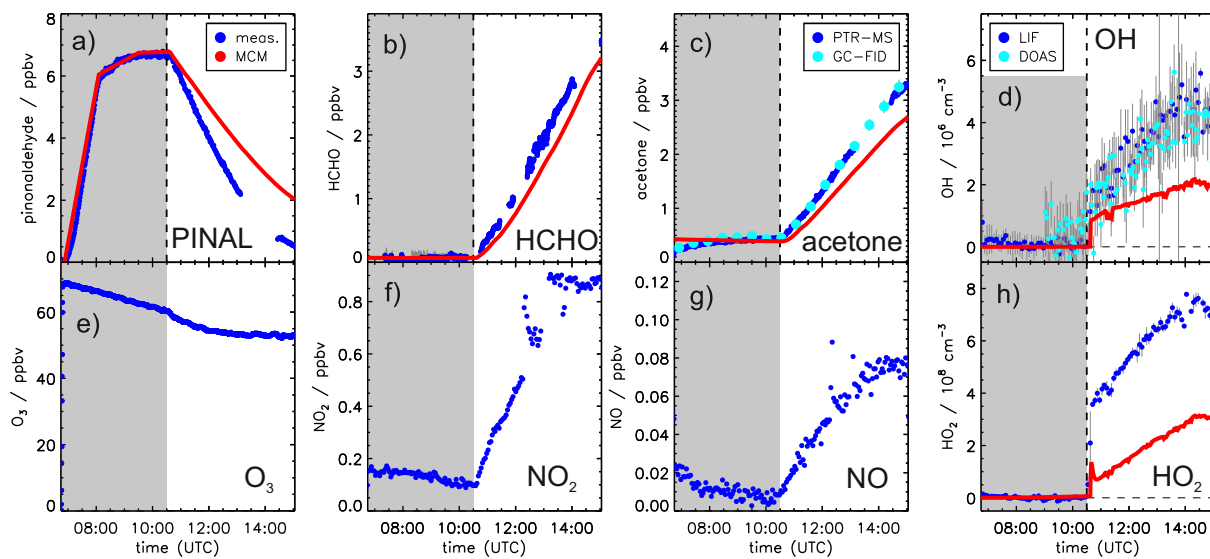
Figure 3. Measured and modeled trace gas concentrations during the photooxidation of pinonaldehyde without OH scavenger. In this experiment, pinonaldehyde is removed by photolysis and reaction with OH. Measured O_3, NO_2 and NO were used as constraints for the model. Grey shaded areas indicate times when the chamber roof was closed.
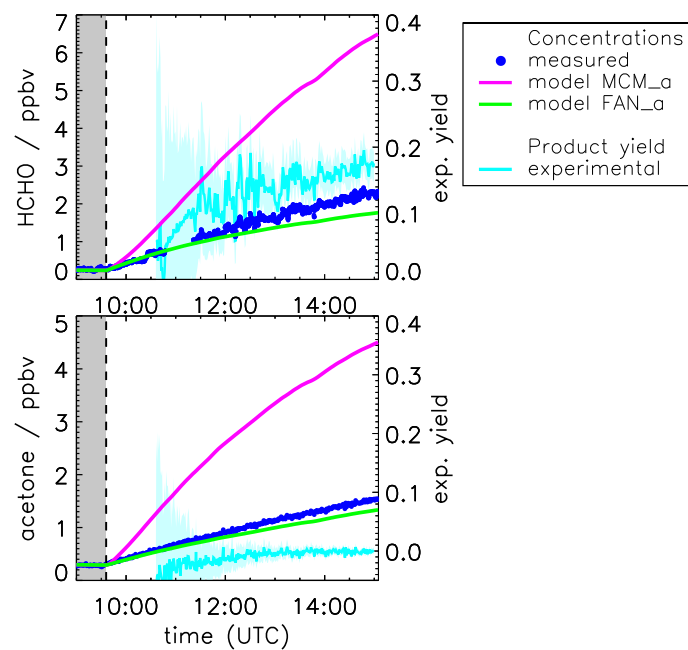
Figure 4. Measured and modeled formaldehyde and acetone mixing ratios for the experiment with OH scavenger. All model runs were done with measured photolysis frequencies for pinonaldehyde (see Fig. 6). Model runs include the MCM and the MCM with additions described in Fantechi et al. (2002). In addition, yields calculated from measured time series are shown (see text for details) with the 1σ error derived from measurements and errors of the applied correction. Colored areas give the uncertainty of this calculation. The additional error caused by the uncertainty of the chamber source is not included here.
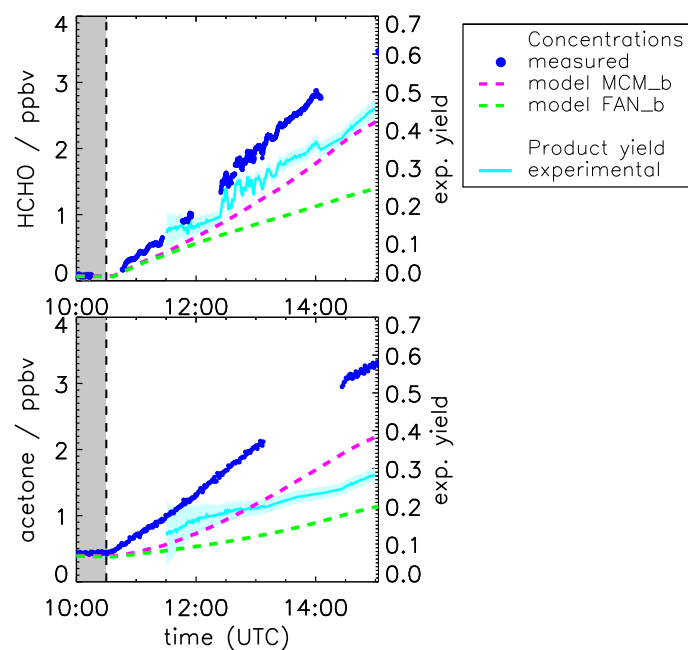
Figure 5. Measured and modeled formaldehyde and acetone mixing ratios for the experiment without OH scavenger. All model runs were done with measured photolysis frequencies for pinonaldehyde and with HO_2 constrained to measurements (see Fig. 7). Model runs were done using the MCM and the MCM with modifications described in Fantechi et al. (2002). In addition, yields calculated from measured time series are shown (see text for details) with the 1σ error derived from measurements and errors of the applied correction. Colored areas give the uncertainty of this calculation. The additional error caused by the uncertainty of the chamber source is not included here.
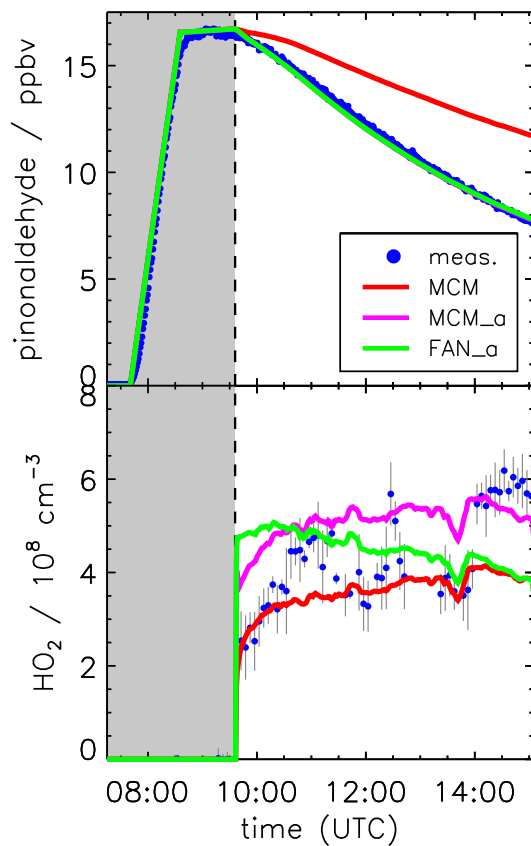
Figure 6. Pinonaldehyde and HO_2 time series during the experiment with OH scavenger. Model runs were done either using the MCM with parameterization of pinonaldehyde photolysis frequencies (MCM), with measured values for photolysis frequencies (MCM_a, see text for details) or with modifications described in Fantechi et al. (2002) (FAN_a). The pinonaldehyde concentration time profile is the same for both model runs MCM_a and FAN_a. Grey shaded areas indicate times when the chamber roof was closed.
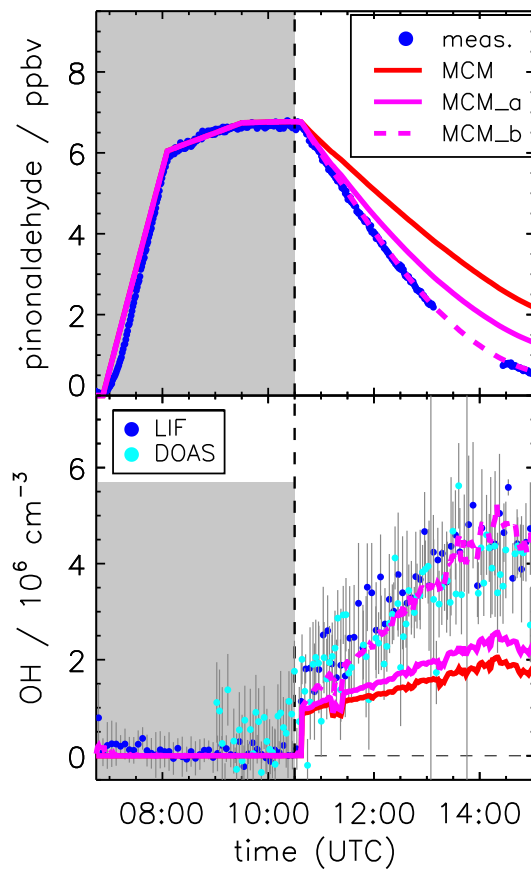
Figure 7. Pinonaldehyde and OH time series during the experiment without OH scavenger. Model runs were done either using the MCM with parameterization of pinonaldehyde photolysis frequencies (MCM) or with measured values for photolysis frequencies (MCM_a, see text for details). The model MCM_b was additionally constrained to measured HO_2 concentration, resulting in an agreement between modeled and measured (LIF and DOAS) OH concentrations. Grey shaded areas indicate times when the chamber roof was closed.
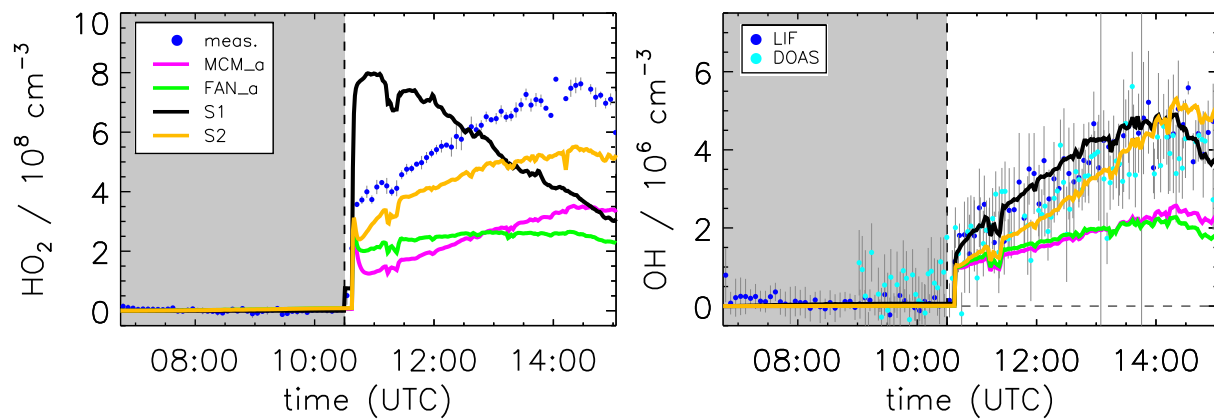
Figure 8. Model sensitivity study of the impact of potential additional HO_2 formation by unimolecular RO_2 reactions (S1) or photolysis of pinonaldehyde oxidation products (S2) compared to the model base case (MCM_a) and the case using the mechanism by Fantechi et al. (2002) (FAN_a). See Table 2 for differences in the model runs. Grey shaded areas indicate times when the chamber roof was closed.